Cerebral Cortex, November 2016;26: 4282–4298

doi: 10.1093/cercor/bhw216
Advance Access Publication Date: 13 September 2016
Original Article

ORIGINAL ARTICLE

Reelin Regulates the Maturation of Dendritic Spines, Synaptogenesis and Glial Ensheathment of Newborn Granule Cells

Carles Bosch[1,2,3,‡], Nuria Masachs[1,2,‡], David Exposito-Alonso[1], Albert Martínez[1], Cátia M. Teixeira[1,2], Isabel Fernaud[2,4,5], Lluís Pujadas[1,2,3], Fausto Ulloa[1,2], Joan X. Comella[2,3,6], Javier DeFelipe[2,4,5,†], Angel Merchán-Pérez[2,4,7,†], and Eduardo Soriano[1,2,3,8,†]

[1]Developmental Neurobiology and Regeneration Unit, Department of Cell Biology, Parc Científic de Barcelona and Institute of Neurosciences, University of Barcelona, Barcelona 08028, Spain, [2]Centro de Investigación Biomédica en Red sobre Enfermedades Neurodegenerativas (CIBERNED), Instituto de Salud Carlos III, Madrid 28031, Spain, [3]Institut de Recerca de l'Hospital Universitari de la Vall d'Hebron (VHIR), Barcelona 08023, Spain, [4]Laboratorio Cajal de Circuitos Corticales, Centro de Tecnología Biomédica, Universidad Politécnica de Madrid, Campus de Montegancedo, Madrid 28223, Spain, [5]Instituto Cajal (Consejo Superior de Investigaciones Científicas), Madrid 28002, Spain, [6]Institut de Neurociències, Departament de Bioquímica i Biologia Molecular, Facultat de Medicina, Universitat Autònoma de Barcelona, Bellaterra 08193, Spain, [7]Departamento de Arquitectura y Tecnología de Sistemas Informáticos, Escuela Técnica Superior de Ingenieros Informáticos, Universidad Politécnica de Madrid, Madrid 28660, Spain, and [8]Institució Catalana de Recerca i Estudis Avançats Academia, Barcelona 08010, Spain

Address correspondence to Eduardo Soriano, Javier DeFelipe and Angel Merchán-Pérez Email: esoriano@ub.edu, defelipe@cajal.csic.es or amerchan@fi.upm.es

[†]JDF, AM and ES are co-senior authors.

[‡]CB and NM authors contributed equally.

Abstract

The Reelin pathway is essential for both neural migration and for the development and maturation of synaptic connections. However, its role in adult synaptic formation and remodeling is still being investigated. Here, we investigated the impact of the Reelin/Dab1 pathway on the synaptogenesis of newborn granule cells (GCs) in the young-adult mouse hippocampus. We show that neither Reelin overexpression nor the inactivation of its intracellular adapter, Dab1, substantially alters dendritic spine numbers in these neurons. In contrast, 3D-electron microscopy (focused ion beam milling/scanning electron microscope) revealed that dysregulation of the Reelin/Dab1 pathway leads to both transient and permanent changes in the types and morphology of dendritic spines, mainly altering mushroom, filopodial, and branched GC spines. We also found that the Reelin/Dab1 pathway controls synaptic configuration of presynaptic boutons in the dentate gyrus, with its

dysregulation leading to a substantial decrease in multi-synaptic bouton innervation. Lastly, we show that the Reelin/Dab1 pathway controls astroglial ensheathment of synapses. Thus, the Reelin pathway is a key regulator of adult-generated GC integration, by controlling dendritic spine types and shapes, their synaptic innervation patterns, and glial ensheathment. These findings may help to better understanding of hippocampal circuit alterations in neurological disorders in which the Reelin pathway is implicated.

Significance Statement: The extracellular protein Reelin has an important role in neurological diseases, including epilepsy, Alzheimer's disease and psychiatric diseases, targeting hippocampal circuits. Here we address the role of Reelin in the development of synaptic contacts in adult-generated granule cells (GCs), a neuronal population that is crucial for learning and memory and implicated in neurological and psychiatric diseases. We found that the Reelin pathway controls the shapes, sizes, and types of dendritic spines, the complexity of multisynaptic innervations and the degree of the perisynaptic astroglial ensheathment that controls synaptic homeostasis. These findings show a pivotal role of Reelin in GC synaptogenesis and provide a foundation for structural circuit alterations caused by Reelin deregulation that may occur in neurological and psychiatric disorders.

Key words: adult neurogenesis, 3D-electron microscopy, FIB/SEM, axospinous synapses, glia

Introduction

Adult neurogenesis in the dentate gyrus (DG) has been implicated in spatial learning and pattern separation (Clelland et al. 2009; Aimone et al. 2011; Sahay et al. 2011), and recently it has been suggested to add flexibility in memory through the forgetting process (Akers et al. 2014). Moreover, impairment of adult neurogenesis has been shown to occur in neurodegenerative and psychiatric diseases (Zhao et al. 2008; Kheirbek et al. 2012; Yu et al. 2014). Whereas recent studies have identified key factors for the regulation and proliferation rates of neuroprogenitor cells (Lie et al. 2005; Jessberger et al. 2008; Lagace et al. 2008; Gao et al. 2009; Karalay et al. 2011; Vadodaria and Gage 2014), much less is known about the mechanisms that control synaptogenesis of adult-generated granule cells (GCs) and their recruitment into adult circuits (Toni et al. 2007). Interestingly, spatial learning accelerates the integration of newborn neurons (Lemaire et al. 2012), and environmental enrichment influences the morphology of their dendritic spines (for simplicity, spines) (Zhao et al. 2014). In turn, Alzheimer's disease murine models show impaired spine maturation in these cells, which is triggered by an unbalanced glutamate/GABA input, among other mechanisms (Sun et al. 2009; Llorens-Martin et al. 2013; Song et al. 2013; Cho et al. 2015).

Reelin is an extracellular protein that is essential for neuronal migration and brain development (D'Arcangelo et al. 1995; Alcantara et al. 1998; Rice and Curran 2001; Soriano and Del Rio 2005; Cooper 2008) and its signaling is mediated by the apolipoprotein E receptor 2 and the very-low-density lipoprotein receptor, which trigger a complex signaling cascade involving the adaptor Dab1 (Howell et al. 1997, 1999; Hiesberger et al. 1999; Beffert et al. 2002; Arnaud et al. 2003; Ballif et al. 2004; Gonzalez-Billault et al. 2005; Simo et al. 2007). Reelin continues to be expressed into adulthood and also regulates dendrite development, the formation of spines, glutamatergic neurotransmission and neural plasticity (Chen et al. 2005; Herz and Chen 2006; Qiu et al. 2006; Groc et al. 2007; Pujadas et al. 2010, 2014; Bosch et al. 2016). Importantly, downregulation of the Reelin pathway, Reelin mutations and genetic variants are implicated in numerous diseases, including Alzheimer's disease, epilepsy, and psychiatric disorders, all involving alterations of hippocampal circuits (Guidotti et al. 2000; Abdolmaleky et al. 2005; Knuesel 2010; Krstic and Knuesel 2013; Pujadas et al. 2014; Dazzo et al. 2015; Moon et al. 2015).

Recently, we found that the Reelin pathway dramatically regulates GC adult neurogenesis; whereas overexpression of Reelin accelerates dendritic maturation, disruption of the Reelin pathway results in aberrant dendritic development and orientation (Teixeira et al. 2012). Here, we investigate the impact of the Reelin pathway in the synaptogenesis of newborn young-adult GCs performing retroviral tracing and 3D-EM (focused ion beam milling/scanning electron microscope (FIB/SEM) technology) (Bosch et al. 2015) and using both gain and loss of function mouse models. We show that the Reelin/Dab1 pathway controls adult GC spinogenesis and synaptogenesis as well as astroglial ensheathment of synapses. These results may have implications in the context of neurodegenerative, psychiatric, and temporal lobe epileptic disorders, in which the Reelin pathway has been implicated (Guidotti et al. 2000; Abdolmaleky et al. 2005; Knuesel 2010; Krstic and Knuesel 2013; Pujadas et al. 2014; Dazzo et al. 2015; Moon et al. 2015).

Materials and Methods

Animals

Conditional knockout Dab1 mice (Dab1-cKO) (Pramatarova et al. 2008) and Reelin-overexpressing (Reelin-OE, gamma strain) (Pujadas et al. 2010) mice were maintained on a C57BL/6J background. Previous work showed that Reelin-OE mice have 2–3 times more Reelin protein (Pujadas et al. 2010), while Dab1-cKO have normal levels of Reelin but its signaling pathway is inactivated (Teixeira et al. 2014). In Reelin-OE mice the Reelin transgene expression is driven by the CaMKII promoter, leading to Reelin expression in pyramidal and GCs. Mutant mice and their littermate controls were housed in groups (2–6 mice per cage) and maintained in a 12 h light/dark cycle with access to food and water ad libitum. All procedures were performed with mice of either sex according to the guidelines of the European Community Directive 2010/63/EU, and were approved by the local ethics committee of the Spanish National Research Council (CSIC) and by the Ethics Committee for Animal Experimentation (CEEA), University of Barcelona (Barcelona, Spain).

Production and Intrahippocampal Injection of High-titer Retrovirus

We used a CAG-GFP retrovirus (RV) stock encoding for GFP and CAG-GFP-IRES CRE encoding for GFP and Cre-recombinase (Zhao et al. 2006) (a generous gift from Fred H. Gage, Salk Institute, CA, USA). To visualize PSD95 clusters in newborn GCs, we used the retroviral vector MRSVPSD95 and Cre-recombinase (Kelsch et al. 2008). RVs were produced by transient transfection of HEK 293 T

cells as described previously (Zhao et al. 2006). RV stocks were concentrated to working titers of 1×10^7–2×10^8 pfu/ml, by means of ultracentrifugation. Young-adult mice (7–8 weeks old, $N = 21$ for light microscopy analysis, $N = 9$ for EM analysis) were anesthetized and placed in a stereotaxic frame. The scalp was incised, and holes were drilled in the skull. Injection coordinates (in mm) relative to bregma in the anteroposterior, mediolateral, and dorso-ventral planes were as follows: [−2.0, 1.4, 2.2]. Of the case, 1.5 µL of virus solution per DG was infused at 0.2 µL/min via a glass micropipette.

Tissue Processing, Histology, and Immunohistochemistry

Animals were perfused with 4% paraformaldehyde at 4 or 8 weeks post-injection. The brains were then removed, postfixed, cryoprotected in 30% sucrose, and frozen. Coronal sections (50 µm thick) were cut and fluorescence immunohistochemistry was performed on free-floating sections. For immunodetection of GFP, polyclonal rabbit anti-GFP primary antibody (Invitrogen, 1:1000) and secondary antibody Alexa Fluor 488- (GFP experiment) or 568-conjugated (PSD95 experiment) goat anti-rabbit (1:1000) were used. To counterstain nuclei, the tissue was incubated in DAPI.

Confocal Microscopy, Image Processing, and Quantification

High-resolution confocal image stacks were acquired using a Leica SP5. For GFP experiments, images were acquired at a resolution of 0.068 × 0.068 × 0.13 µm in x,y,z, respectively. Stacks were further deconvolved based on an experimental point spread function using a Wiener algorithm available in Fiji (Schindelin et al. 2012). In PSD95 experiments, the resolution was 0.077 × 0.077 × 0.5 µm. For both experiments, MosaicJ plug-in from Image J (NIH) was used to obtain whole neuron images, allowing us to determine the 3 sublayers of the Molecular Layer (ML) (Inner molecular layer (IML), middle molecular layer (MML), and outer molecular layer (OML)). For each genotype, age, and layer, 2 or 3 dendritic segments of 20–30 µm were analyzed per neuron (13–21 neurons per animal, 2–5 animals per condition/age). In the GFP experiment, spines were counted using Imaris (Bitplane). In the PSD95 experiment, a semi-automatic system using an intensity threshold was used in order to count PSD95-GFP spots. The length of the respective segment of the dendritic arbor was then measured to obtain the densities. Comparisons among groups were performed using a two-way ANOVA followed by Holm-Sidak's post hoc test. All values are reported as the mean ±SEM.

EM Tissue Preparation

At 3–4 and 8–9 weeks after viral injection, mice ($N = 9$) were anesthetized by isofluorane inhalation and processed for EM as previously described (Bosch et al. 2015). Briefly, mice were intracardially perfused with 4% paraformaldehyde and 0.1% glutaraldehyde in 0.12 M phosphate buffer and the brain was postfixed overnight in 4% paraformaldehyde. Of the case, 100 µm thick vibratome slices were permeabilized by freeze-thawing, immunostained with a rabbit polyclonal anti-GFP antibody (1:1000), a biotinylated goat anti-rabbit secondary antibody, and the ABC-peroxidase kit (Vector Labs), and then developed with DAB and hydrogen peroxide. Slices were postfixed in 2% osmium tetroxide, incubated in 2% uranyl acetate, and flat-embedded in Araldite. DAB-labeled cells were identified under light microscopy and optimal dendritic segments were chosen (Bosch et al. 2015). The blocks were then trimmed so that the selected segments remained at 3–5 µm below the block surface.

FIB/SEM Imaging

Blocks were glued on stubs and the ensemble conductivity was enhanced by silver-painting the block sides and by sputter-coating the block face with gold/palladium (Merchan-Perez et al. 2009). Automated serial imaging and slicing of the samples was carried with a FIB/SEM (Crossbeam Neon40 EsB, Carl Zeiss NTS GmbH, Oberkochen, Germany). A secondary electron image of the block surface provided useful landmarks that allowed an accurate overlay of the scene with the previously acquired LM images, and therefore permitted the fine prediction of the location of the dendrite of interest (Bosch et al. 2015). After milling a coarse trench with a 10 nA gallium beam, the recently cut surface was explored using a backscattered electron detector. Then the final framing was chosen according to the exact location of the dendrite of interest. Serial milling and imaging cycles followed, providing stacks of images, each representing a high-resolution 3D sample (Merchan-Perez et al. 2009; Bosch et al. 2015). Milling involved a beam current of 750 pA. Images of the recently cut surface were obtained by scanning the block surface with a 1.7 kV, 1.2 nA electron beam, and recording the signal with an in-column energy-selective backscattered electron detector. Dwell time was set to 100 ns/pixel, and images were line-averaged 4 times. Pixel sizes were set at 3.7 nm (except for 2 stacks, in which pixel size was 4.0 and 5.0 nm, respectively). Z-axis resolution (cutting thickness) was 25 nm (except for 1 stack: 20 nm). Voxel dimensions were carefully stored for each stack and applied before any further measurement. Images typically covered a field of view (FOV) of 7.6 × 5.7 µm, although in one case a larger FOV of 11.4 × 8.5 µm was chosen. These settings allowed the acquisition of enough detail and neuropil at a fast scanning cycle (combined scan-milling cycle times of ~3 min), thereby allowing the milling and imaging of large volumes (average of 5.5 µm in depth).

Stacks acquired from Reelin-OE mice (7 stacks at 3/4 weeks and 2 stacks at 8 weeks, average 167 μm^3 of imaged tissue per stack) and from Dab1-cKO mice (2 at 4 weeks and 3 at 8/9 weeks, average 227 μm^3), were compared with image stacks comprising labeled dendritic segments from control, wild-type (WT) mice of labeled 3–4, and 8- to 9-week-old GCs (Bosch et al. 2015). All the experiments in Reelin models and WT mice were run and analyzed in bulk.

Analysis of Connectivity

Image post-processing involving rigid registration (no rotation) and signal normalization across slices were performed with Fiji (Schindelin et al. 2012). Each spine, synapse, and afferent axonal bouton was annotated in a database, which allowed systematic review by at least 3 independent specialized scientists. Spines were classified into 5 categories according to their key morphological features (Harris et al. 1992; Rochefort and Konnerth 2012; Bosch et al. 2015): filopodial, thin, stubby, mushroom, and branched. Long and thin spines with a pointed PSD, with similar diameters in the neck and head were classified as "filopodia"; small necks tipped by small round heads were classified as "thin"; short thick spines with no size differences between neck and head and spine length similar to neck width were classified as "stubby"; spines tipped by large heads typically displaying U-shapes were classified as "mushroom";

and spines with more than 1 head arising from a single neck were classified as "branched".

All presynaptic boutons establishing synapses onto labeled spines were identified and we annotated the total number of synapses they established (including those with unlabeled spines) (Bosch et al. 2015). In addition, we analyzed the connectivity of presynaptic boutons surrounding labeled dendrites but establishing contact exclusively with non–GFP-positive elements. In these 4- to 5-month-old mice, these synaptic non-labeled spines were assumed to arise from mature, fully integrated GCs, and thus these boutons were termed "mature". A random selection of 33–65 boutons (per animal) contacting non-labeled spines was analyzed, providing a complete representation of the afferent connectivity to mature GCs ($N = 378$ boutons for WT, $N = 355$ boutons for Reelin-OE).

Segmentation and Quantitative Analysis

Segmentation of labeled dendrites, afferent boutons, and synaptic contacts was performed semiautomatically with EspINA (Morales et al. 2011; Bosch et al. 2015). Imaris (Bitplane) was used to generate and edit 3D meshes from segmented images, and to extract morphometric measurements from these elements. Spines were cut from the dendritic shaft. Branched spines were further cut into individual spines at their shared neck isthmus. From each mesh representing a fully 3D-reconstructed spine and synapse we measured, as previously described (Bosch et al. 2015), the following parameters: Spine volume and surface, spine sphericity, synapse size and surface, and synapse sphericity. Pooled data from all elements from each group were compared between genotypes of the same age performing Kruskal–Wallis tests with post hoc Dunn's multiple comparisons tests, unless stated otherwise. For comparisons between two groups we applied the Mann–Whitney test.

Analysis of Astroglial Ensheathment

Identification of perisynaptic astrocytic processes (PAPs) was made exploring the 3D image datasets in Fiji. Astrocytic processes were identified by the sinuous morphology of the processes, the lack of microtubule bundles, and their pale cytoplasm (Peters and Palay 1991). We determined the proportion of ensheathed presynaptic and postsynaptic partners on synapses from newborn GCs (127 spines and 123 boutons for WT, 96 spines and 79 boutons for Reelin-OE, and 82 spines and 66 boutons for Dab1-cKO). Completely imaged spines and boutons in 3D (stacks of FIB/SEM images) were analyzed every 4 slices (100 nm) (115 spines and 114 boutons for WT; 84 spines and 71 boutons for Reelin-OE; and 64 spines and 54 boutons for Dab1-cKO). For each spine and its presynaptic bouton we traced the contours of all synaptic elements, evaluated the presence of glial ensheathment and measured the perimeter of the synaptic elements that were enwrapped by glial processes, with respect to the total perimeter. Statistical analysis involved Kruskal–Wallis test with post hoc Dunn's test for comparisons between genotypes of the same age, and Mann–Whitney test for comparisons between two groups.

Results

Regulation of Dendritic Spine Development in Young-adult Born GCs by the Reelin/Dab1 Pathway

To investigate the role of Reelin on GC synaptogenesis, we injected GFP RV constructs into the DG of young-adult WT and Reelin-OE mice (Pujadas et al. 2010; Teixeira et al. 2012). To study the influence of Reelin downregulation, we inactivated Dab1 in adult neuroprogenitor cells by injecting Dab1-cKO mice with RV constructs expressing Cre and GFP, thus allowing us to monitor the effect of cell-autonomous inactivation (Teixeira et al. 2012). Dab1 is an essential component of the Reelin cascade and its inactivation results in a phenocopy of Reelin-deficient mice (Sheldon et al. 1997; Franco et al. 2011; Teixeira et al. 2012). WT mice injected with GFP and Cre RV were used as controls (Fig. 1*a*). The density of spines was analyzed at 4 and 8 weeks post-injection in the 3 sublayers of the ML which receive differential inputs from the entorhinal and the commissural/associational pathways (Andersen et al. 2007). We found that in WT mice there was an overall increase in the density of spines between 4 and 8 weeks (IML: 27.39%; MML: 25.57%; OML: 14.50%; Fig. 1*b*,*d*). The overexpression of Reelin did not alter the densities of spines at any time point, compared with WT mice, although differences between 4 and 8 weeks were observed just in the IML (increase of 18.53%; Fig. 1*b*,*d*). In contrast, we found that Dab1-inactivated GCs displayed a transient increase in the density of spines at 4 weeks, with spine numbers being similar to WT mice at 8 weeks (Fig. 1*b*,*d*).

We next took advantage of RV vectors expressing PSD95-GFP to map the onset of input synapses. Injections of such retroviral vectors delineated dendrites and spines, which were tipped with PSD95-GFP clusters corresponding to synaptic puncta (Fig. 1*c*). These results confirmed the increase in synaptic puncta in WT mice between 4 and 8 weeks, as well as in Reelin-OE mice, but without differences between these 2 genotypes. Cell-autonomous Dab1 inactivation resulted in a moderate, transient increase in PSD95-positive puncta at 4 weeks (Fig. 1*c*,*e*). Interestingly, Dab1-inactivated GCs extended ectopic, basal dendrites into the hilus (Teixeira et al. 2012), which were also covered by a high density of spines tipped with PSD95-GFP positive puncta (1.1 spots/μm at 4 w and 1.37 spots/μm at 8 weeks), suggesting that ectopic GC dendrites have spine densities similar to apical dendrites. Thus, by using both gain- and loss-of-function models and 2 different retroviral markers we concluded that the Reelin pathway appears not to regulate either the developmental program or the numbers of spines and synaptic contacts in young-adult-born GCs, except for a transient increase in Dab1-deficient GCs.

The Reelin/Dab1 Pathway Regulates the Shapes of Dendritic Spines in Newborn GCs

We next addressed spine synaptogenesis in RV-traced GCs by using FIB/SEM technology, which allows high-throughput 3D-EM reconstructions of spines and synapses with high resolution. We reconstructed a total of 14 dendritic segments from Reelin-OE mice and Dab1-inactivated neurons, allowing complete 3D reconstruction of up to 195 spines (4 weeks: 45 Reelin-OE, 27 Dab1-cKO; 8–9 weeks: 82 Reelin-OE, 41 Dab1), which were compared with WT young-adult generated GC dendrites (Bosch et al. 2015). Together with the control group, the study includes a total of 443 spines. These 3D reconstructions allowed us to trace identified spines back to the parent dendrites and to study the 3D architecture of synaptic interactions including presynaptic elements (Movie 1, Figs. 2 and 3). As in WT mice, most GC spines were contacted by a single presynaptic bouton in both Reelin-OE and Dab1-cKO mice establishing asymmetric synapses, although a small percentage lacked synaptic contacts (non-synaptic spines, Dab1-cKO: 1 (3%) at 4 weeks and 3 (6%) at 9 weeks; Reelin-OE: none at 4 weeks and 3 (6%) at 8 weeks). The

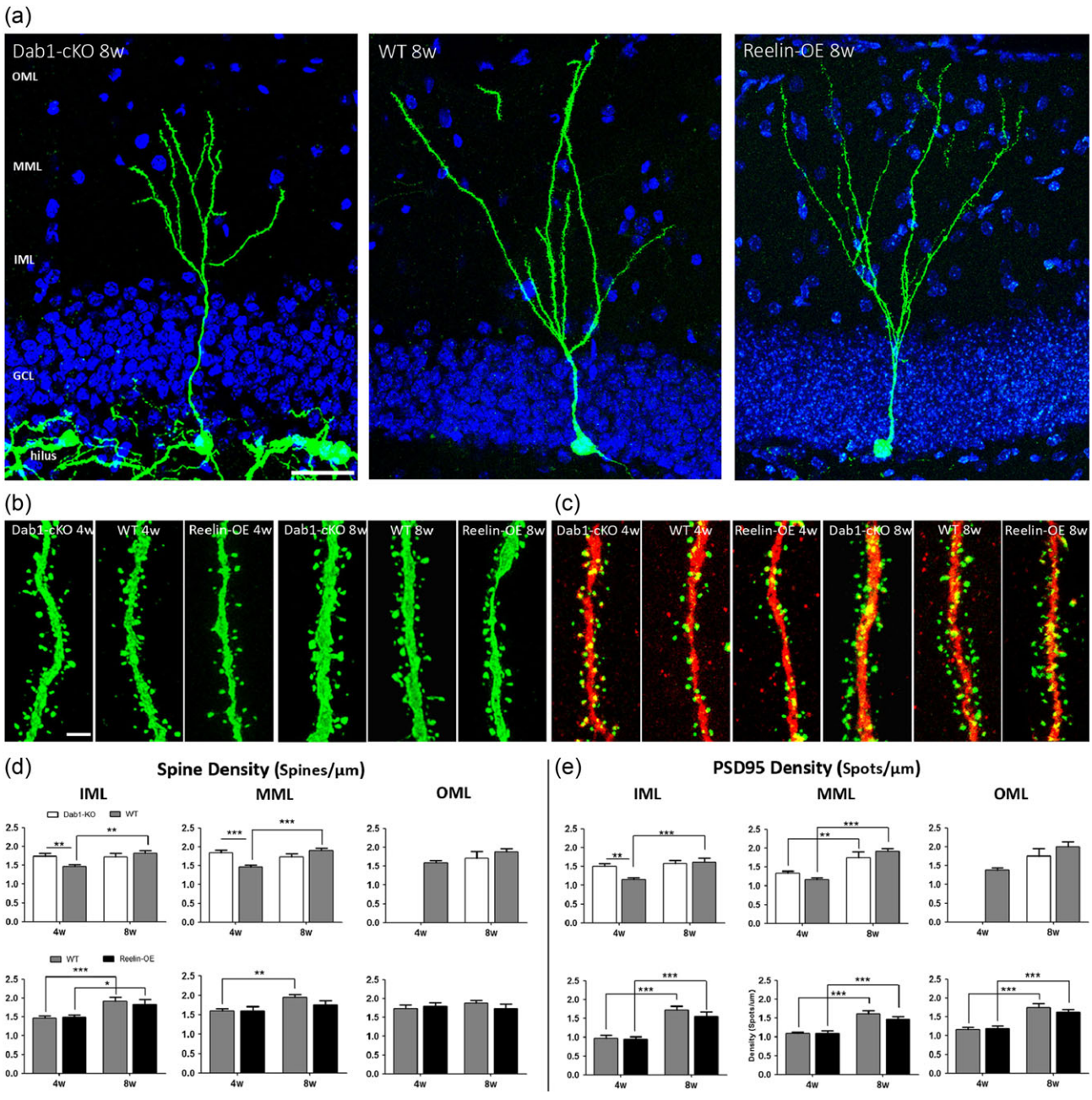

Figure 1. Density of spines and postsynaptic densities remain largely unaltered in Reelin-OE and Dab1-cKO newborn GCs. (*a*) Representative images of GFP-labeled young-adult-born neurons from Dab1-cKO, WT, and Reelin-OE mice at 8 weeks. (*b* and *c*) Representative examples of dendritic segments analyzed from adult-born neurons expressing GFP (*b*) and PSD95-GFP (*c*) from Dab1-cKO, WT, and Reelin-OE mice at 4 and 8 weeks. (*d* and *e*) Quantifications of the spine density (*d*) and PSD95-GFP spot density (*e*) in dendritic segments of newborn neurons in the 3 ML layers. Scale bar = 50 µm (*a*) and 2 µm (*b* and *c*). Abbreviations: GCL, Granule Cell Layer. Data represented as mean ± SEM; $^{*}P < 0.05$; $^{**}P < 0.01$; $^{***}P < 0.001$.

vast majority of spines received synaptic input on their heads in all groups studied.

The same 5 main types of spines observed in our previous analysis on WT GC spinogenesis (filopodial, thin, stubby, mushroom, and branched, Bosch et al. 2015) were identified in Reelin-OE and Dab1-deficient mice, although stubby spines were only occasionally found in these phenotypes. Several examples, corresponding to mushroom, filopodial, branched, and thin spines, are shown in Figs. 2 and 3. To analyze the impact of the Reelin/Dab1 pathway in GC dendritic spinogenesis, we compared the percentages of spine types among the different genotypes (Fig. 4*a*,*b*). At 4 weeks in WT mice, the largest percentage of spines corresponded to the thin (48%) and the mushroom and filopodial categories (24%; Fig. 4*b*). At this time point, Reelin-OE mice displayed a marked increase in mushroom spines (53%), concomitant with a decrease in filopodial spines (−57%) when compared with WT. The percentage of mushroom and branched spines was also increased in Dab1-inactivated dendrites (64% and 257%, respectively), at the expense of a reduction in thin spines (−55%, Fig. 4*b*). At 8 weeks in WT mice, the percentages of mushroom, filopodial and thin spines were roughly similar (although slightly reduced) to those

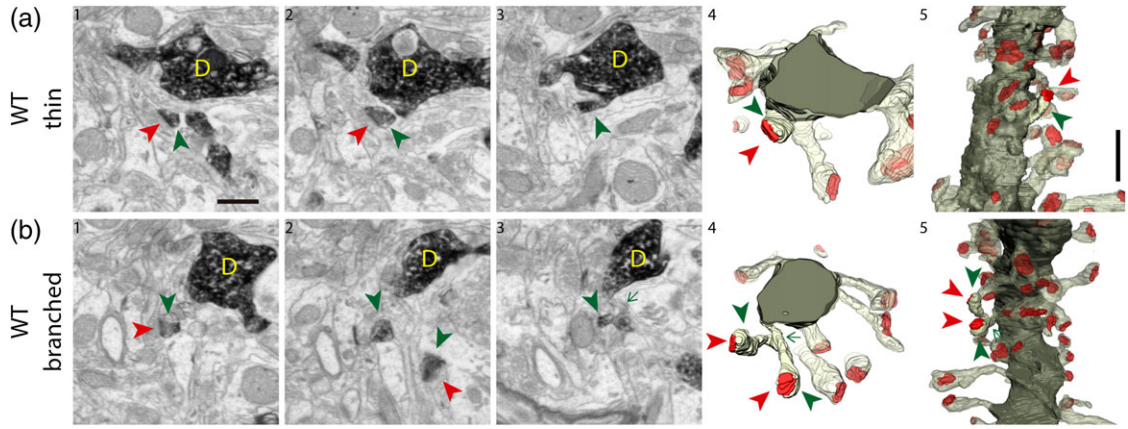

Figure 2. Spines of 8-week-old WT GFP/DAB-labeled GCs reconstructed with FIB/SEM microscopy. Examples of a thin (*a*) and a branched (*b*) spine arising from their parent dendrite (D). The left images (1–3) show selected serial planes of the spines depicting the head (green arrowheads), neck (green arrow) and synaptic contact (red arrowheads). The right 3D reconstructions (4–5) show the labeled spines in 2 orthogonal orientations. The dendritic shaft is shown in solid dark green, the spine of interest in solid pale green, and its synapse in solid red. Neighboring spines and synapses are indicated in light pale green and red, respectively. Scale bar in *a1* is 0.5 μm and applies to *a*-*b* 1–4. Scale bar in *a*5 is 1 μm and applies to *a*-*b*5. Abbreviations: *D*, dendrite.

of 4-week-old neurons. In contrast, the presence of both branched and stubby spines was almost exclusive of this stage (Fig. 4*b*). The main change observed in 8-week-old neurons in Reelin-OE mice, compared with WT mice, was an increase in the percentage of mushroom and filopodial spines (40% and 28%, respectively). Conversely, Dab1-inactivated dendrites exhibited a marked decrease in the percentage of mushroom spines (−53%), accompanied by an increase in filopodial spines (113%; Fig. 4*b*). Together, these results indicate that although some GC spine types (mushroom, filopodial, and thin) are fixed and robust in WT mice already at 4 weeks, branched and stubby spines are a distinctive feature of mature 8-week-old GCs (Bosch et al. 2015). Moreover, whereas the overexpression of Reelin leads to an increase in mushroom spines at 4 and 8 weeks, Dab1 inactivation leads to profound changes, both transient and permanent, in spine shapes, with a transient increase in mushroom and branched spines at 4 weeks, followed by a marked decrease in mushroom spines at 8 weeks, accompanied by an increase in the filopodial type (Fig. 4*b*).

We next performed a morphometric 3D analysis of the fully reconstructed spines and synapses. Sizes of spines and synapses (measured either via their respective volumes or enveloping surfaces) were distributed in a right-skewed curve, whereas their sphericities were distributed symmetrically around the mean. All these parameters displayed a continuum in their values, as previously described (Arellano et al. 2007; Benavides-Piccione et al. 2013; Bosch et al. 2015). Whereas at 3–4 weeks spines from WT neurons were less spherical than the other 2 experimental groups, the opposite held true at 8–9 weeks (Fig. 4*c*). This proves that spines are more irregularly shaped in 8–9 weeks Reelin-OE and Dab1-cKO neurons, and suggests that spine structural maturation is affected by the Reelin signaling. Synapse sphericity was smaller in Reelin-OE mice at 8–9 weeks, indicating greater complexity (Fig. 4*d*).

At 4 weeks, all groups displayed similar spine sizes (Fig. 4*e* and Supplementary Fig. 1*a*). At 8–9 weeks, in turn, spines of Reelin-OE mice were 51% larger than controls. This increase was driven exclusively by the spines having volumes above 3.0E7 nm^3 (surfaces above 1.0E6 nm^2), which accounted for half of the spine population in both the control and Reelin-OE groups (WT: 111 spines, 49.1%; Reelin-OE: 42 spines, 51.2%). No differences were found between WT and Dab1-cKO spine volumes (Fig. 4*f*,g and Supplementary Fig. 1*b*). We next analyzed sizes of the 3D-reconstructed synaptic contacts. At 3–4 weeks synapses were similar across all groups (Fig. 4*h* and Supplementary Fig. 1*d*). At 8–9 weeks, we found that the Reelin/Dab1 pathway positively regulated the size of synaptic contacts (Fig. 4*h*,i and Supplementary Fig. 1*d*,*e*). Similarly to the previous observations, the changes in synaptic size were driven by specific synapse pools, with the synapses larger than 3.3E6 nm^3 (2.0E5 nm^2) showing larger values in Reelin-OE mice (WT: 125 synapses 56.8% of the population; Reelin-OE: 42 synapses, 61.7%). The synapses smaller than this threshold were the only ones showing lower values in Dab1-cKO samples (WT: 95 spines, 43.2%; Dab1-cKO: 26 spines, 65%) (Fig. 4*i*–*k*). Altogether, these findings indicate that spines exhibited abnormal sphericities at both time points in both Reelin experimental groups, and increased spine sizes in Reelin-OE (and smaller sizes in Dab1-cKO neurons), suggesting an increase in synaptic complexity concomitant with Reelin dosage.

The Reelin/Dab1 Pathway Regulates the Innervation of Young-adult-Generated GCs by Multi-Synaptic Axon Terminals

In the DG, axonal boutons establishing synapses with spines of newborn GCs often contact additional, unlabeled spines (multiple synaptic boutons, MSBs), which have been suggested to enhance synchronicity of the newborn GC with the pre-existent circuitry (Harris 1995; Toni et al. 2007; Bosch et al. 2015). We investigated how the Reelin/Dab1 pathway affected the synaptic features of axon terminals that were presynaptic to labeled GCs. We analyzed the connectivity of a total of 476 terminals innervating identified spines from Reelin-OE (129) and Dab1-inactivated GCs (76), which were compared with WT GCs (271, Bosch et al. 2015). Several examples of MSBs contacting both newborn GC spines and unlabeled spines are shown in Fig. 5*a*–*d*. We found that the percentage of MSBs remained unchanged in all 3 phenotypes at 4 weeks (64–76%), whereas the remaining presynaptic boutons established synapses exclusively onto the GFP-labeled spine (single synaptic boutons, SSBs; Fig. 5*e*,*f*). At 8 weeks, however, the percentage of MSBs was significantly lower in both Reelin-OE and Dab1-

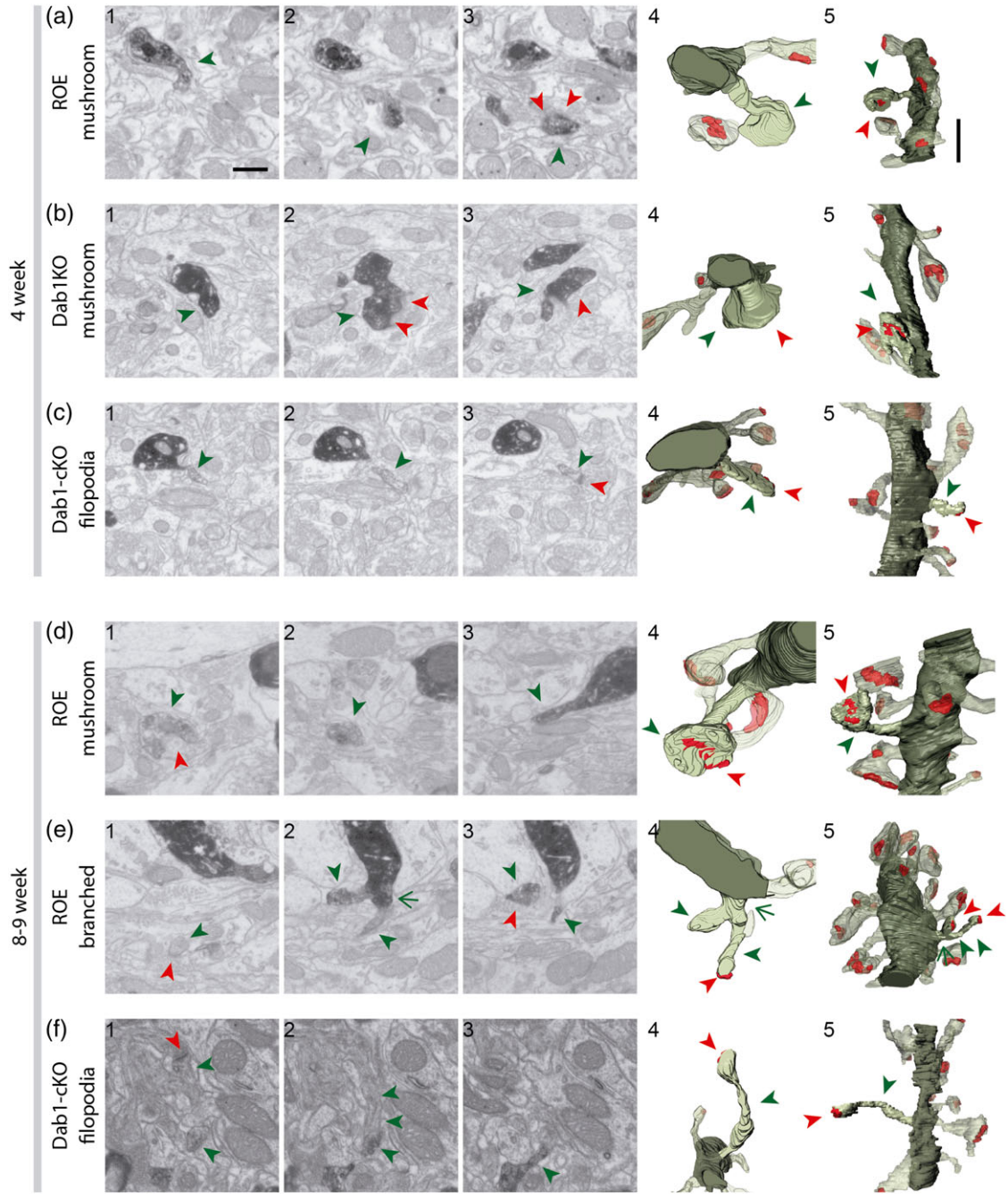

Figure 3. Spines of 8- to 9-week-old Reelin-OE and Dab1-cKO GFP/DAB-labeled GCs reconstructed with FIB/SEM microscopy. Examples of spines of the different reported types arising from dendrites of 4-week (*a*–c) and 8- to 9-week-old (*d*–*f*) Reelin-OE (*a*, d and *e*) and Dab1-cKO (*b* and c, *f*) GCs. Mushroom, branched, and filopodial spines are shown. The left images (1–3) show selected serial planes of the spines depicting the head (green arrowheads), neck and synaptic contact (red arrowheads). The right 3D reconstructions (4–5) show the labeled spines in 2 orthogonal orientations. The dendritic shaft is shown in solid dark green, the spine of interest in solid pale green, and its synapse in solid red. Neighboring spines and synapses are indicated in light pale green and red, respectively. Scale bar in *a*1 is 0.5 μm and applies to *a*–*f* 1–4. Scale bar in *a*5 is 1 μm and applies to *a*–*f*5.

inactivated mice (47% and 53%, respectively) than in WT GCs (72%) (Fig. 5*f*). This notion was also supported by the distribution analyses, showing that only WT neurons had boutons with ≥5 synapses on distinct spines (Fig. 5*e*), and by the average connectivity/bouton, which demonstrated an overall 40% decrease in Reelin-OE (41% less contacts per bouton, 38% less contacts per MSB), and in Dab1-deficient mice (41%, 31%), compared with WT mice (Fig. 5*g*,*h*). Finally, the SSB/MSB ratio analyzes showed that all spine types accounted equally for the decrease in the percentage of MSBs in Reelin-OE and Dab1-inactivated mice (Fig. 5*i*).

These results suggested that synaptic complexity (i.e., number of axo-spinous synapses per bouton) increases in mature, 8-week-old GCs in WT mice, and that such increase is perturbed in both gain- and loss-of-function Reelin models. To substantiate these findings we decided to investigate the synaptic complexity of boutons establishing contacts exclusively with unlabeled spines, the majority of which in 5-month-aged

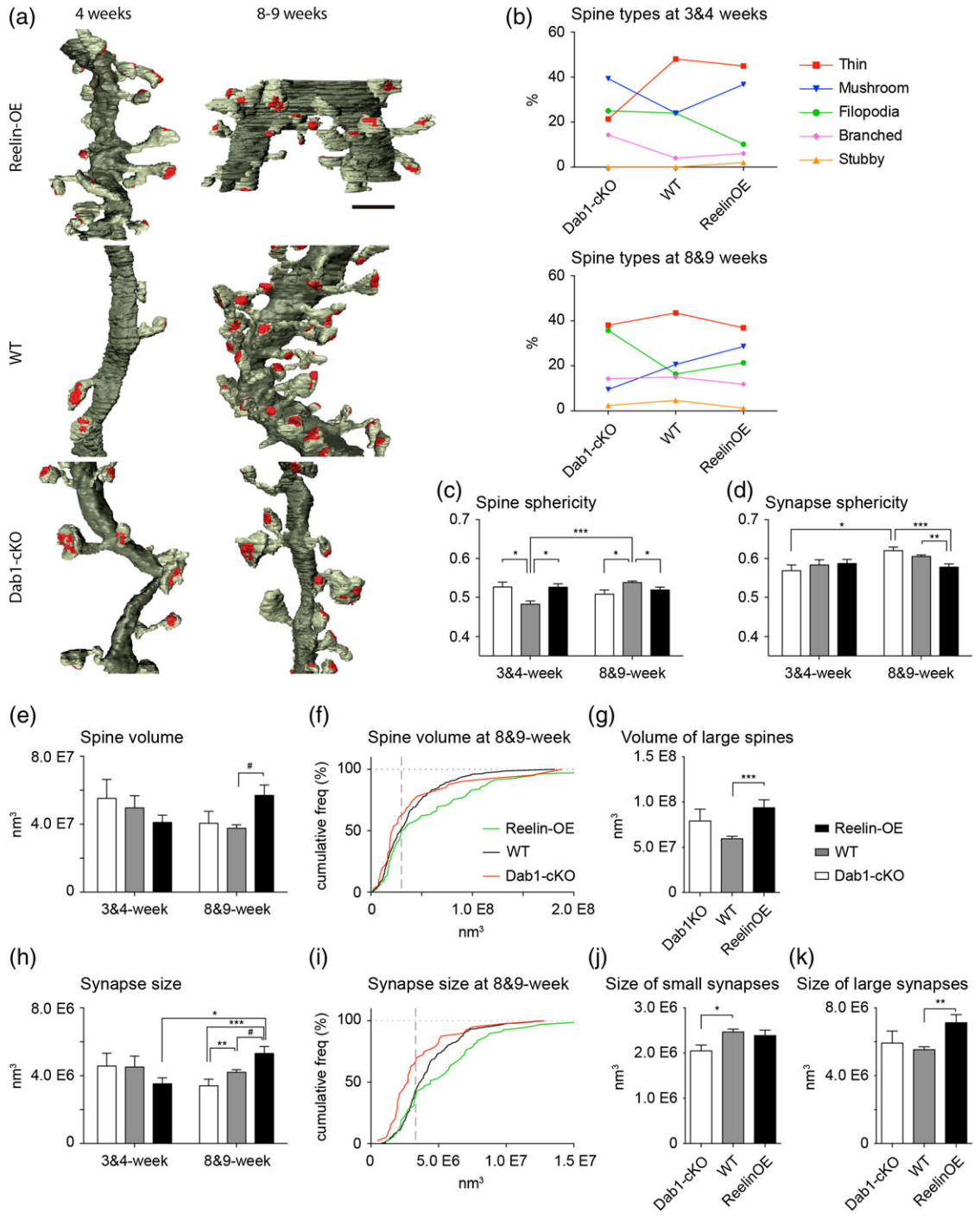

Figure 4. The Reelin/Dab1 pathway alters newborn GC dendritic spine morphology and types. (*a*) 3D reconstructions allowing comparison of dendritic segments and spines at 3–4 and 8–9 weeks. The color code is the same as that described in Fig. 3. (*b*) Plots show the percentages of the different types of spines at 3–4 and 8–9 weeks. (*c* and *d*) Sphericities of fully reconstructed spines (*c*) and synapses (*d*) at the different time points and genotypes. (*e*) Spine volumes of fully reconstructed spines at the different time points and genotypes. (*f*) Cumulative distribution of spine volumes at 8–9 weeks. Notice the threshold (dashed gray line) above which Reelin-OE spine volumes distribute differently from WT. This population of large spines is analyzed in detail in (*g*). (*h*) Synapse sizes of fully reconstructed synapses at the different time points and genotypes. (*i*) Cumulative distribution of synapse sizes at 8–9 weeks. Notice the threshold (dashed gray line) above which Reelin-OE synapses show larger sizes than WT. This threshold was used to split all synapses into 2 groups, the smaller synapses being analyzed in (*j*) and the larger ones in (*k*). Scale bar in *a* is 1 µm. Data represent mean ± SEM. $^{*}P < 0.05$, $^{**}P < 0.01$, $^{***}P < 0.001$; Kruskal–Wallis test and post hoc Dunn's. $^{\#}P < 0.05$; Mann–Whitney test.

mice must correspond to synaptic contacts on mature GCs (Movies 2 and 3). This study was performed in WT and Reelin-OE mice, as Dab1-deficient animals were not suitable because the cre-mediated inactivation was cell-autonomous. Our results showed that both the percentage of MSBs and the average of contacts/bouton were identical to those found in boutons contacting 8-week-old, GFP-labeled GCs (Fig. 5*f*-*h* and Fig. 6), indicating that the synaptic architecture found in 8-week-old neurons is likely to be representative of mature synapses in the ML. Together, these findings indicate that the

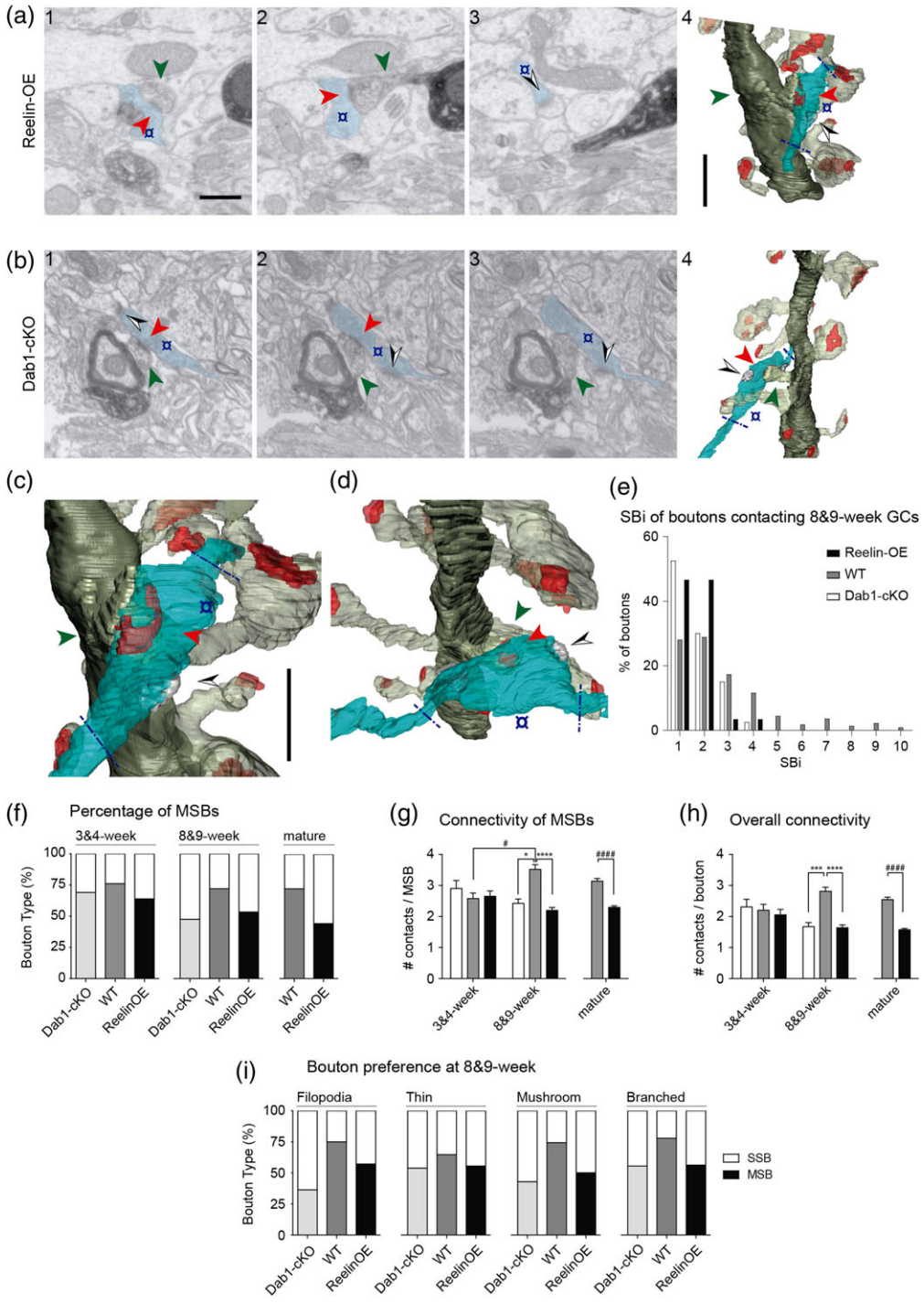

Figure 5. The Reelin/Dab1 pathway strongly regulates presynaptic innervation of newborn GC spines. (*a*–*d*) Two examples depicting multiple synaptic boutons establishing synaptic contacts with Reelin-OE (*a*, *c*) and Dab1-cKO (*b*, *d*) GCs. The left FIB/SEM images (1–3) show selected serial planes of the labeled dendritic spine heads (green arrowhead) and the presynaptic bouton (colored in blue) establishing a synapse onto them (red arrowhead). The boutons establish additional synapses (black and white arrowheads) on non-labeled spines. The right 3D reconstructions (4) show the same elements in a different orientation. Tilted larger magnifications of *a*4, *b*4 are shown in *c*, *d*, respectively. Note that only varicosities presynaptic to the labeled spine were analyzed (delimited by blue dashed lines in the 3D panels). The color code is as described in Fig. 3; additionally, the axon is shown in light blue, and synapses established by the axon on non-labeled spines in solid gray. (*e*) Histogram showing the frequency of synaptic contacts (SBi, number of synapses per bouton) established by axon terminals at 8–9 weeks. (*f*) Percentage of SSB and MSB that make synapses onto dendritic spines aged 3–4 and 8–9 weeks. (*g* and *h*) Average number of synaptic contacts established by MSBs (*g*) and by any bouton (*h*) on 3–4 and 8- to 9-week-old GCs. Values obtained for neighboring "mature" axons are also shown. (*i*) Percentage of SSBs and MSBs establishing contacts on each spine type at 8- to 9-week-old WT, Reelin-OE and Dab1-cKO GCs. Scale bar in *a*1 is 0.5 μm and applies to *a* and *b* 1–3. Scale bar in *a*4 is 1 μm and applies to *a* and *b*4. Scale bar in *c* is 1 μm and applies to *c* and *d*. Data represent mean ± SEM. $^{*}P < 0.05$, $^{***}P < 0.001$, $^{****}P < 0.0001$; Kruskal–Wallis test and post hoc Dunn's. $^{\#}P < 0.05$, $^{\#\#\#\#}P < 0.0001$; Mann–Whitney test.

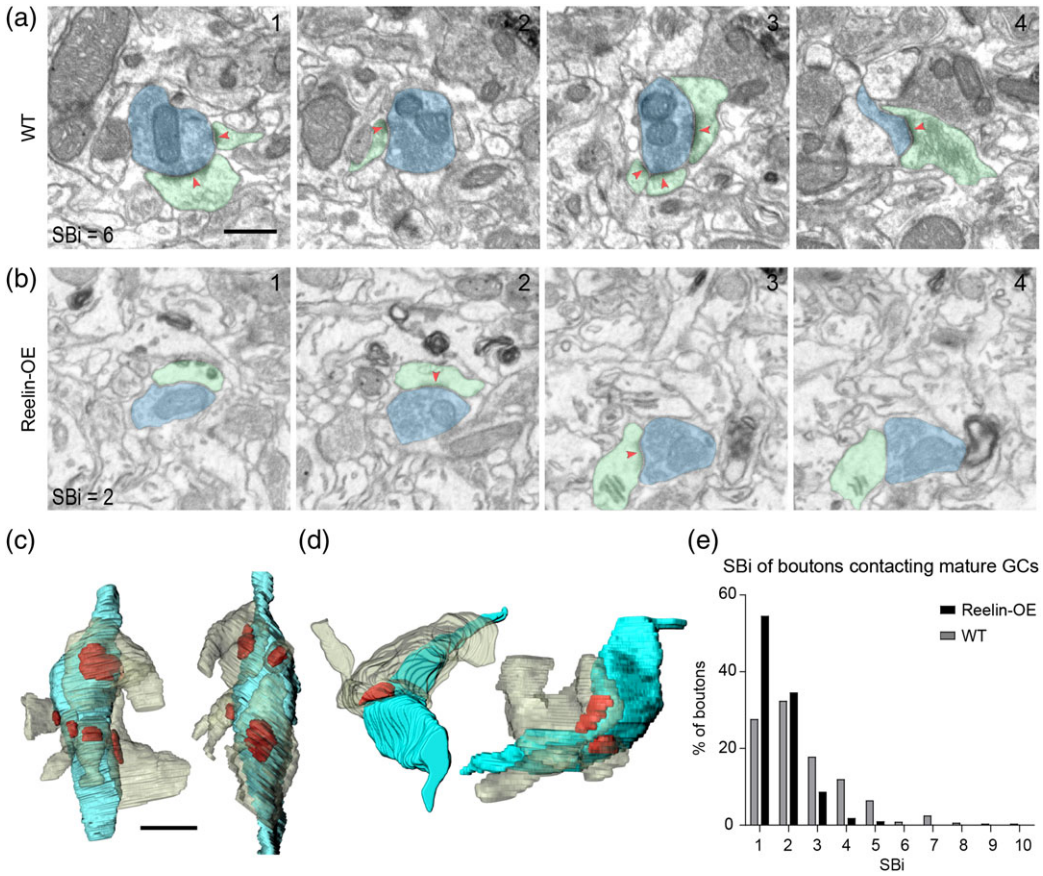

Figure 6. Presynaptic innervation of mature GCs in WT and Reelin-OE neurons. Two examples depicting synaptic boutons establishing multiple synaptic contacts (total number of contacts, SBi, indicated in *a* and *b*1) with mature WT (*a*) and Reelin-OE (*b*) GCs. The EM panels (*a* and *b* 1–4) show selected serial planes of multisynaptic boutons (blue) establishing synapses (red arrowhead) with non-labeled spines (green). (*c* and *d*) 3D reconstructions of the bouton shown in *a* (*c*) and *b* (*d*) in different orientations. (*e*) Histogram showing the frequency of synaptic contacts established by axon terminals on mature GCs. Scale bar in *a* is 0.5 μm and applies to *a* and *b*. Scale bar in c is 0.5 μm and applies to c and d.

Reelin/Dab1 pathway regulates the synaptic complexity of terminals presynaptic to GCs in the DG.

The Reelin/Dab1 Pathway Regulates Astroglial Ensheathment of Newborn GC Synapses

Astroglial ensheathment of synapses is increasingly thought to be important in the control of synaptic neurotransmitter levels, extracellular homeostasis, neuron/glia neurotransmission, and spine development and plasticity (Araque et al. 2014; Bernardinelli et al. 2014a; Haydon and Nedergaard 2015; Krzisch et al. 2015; Martin et al. 2015; Sultan et al. 2015). We next analyzed fully reconstructed GC synapses to address whether the Reelin cascade modulates astroglial ensheathment of synapses established with spines of newborn GC. As shown in the 3D reconstructions in Fig. 7, PAPs were in direct apposition with, and engulfed, both the presynaptic and the postsynaptic elements arising from GFP-traced GCs. The degree of PAP ensheathment was variable, with some synapses being largely enwrapped by PAPs and others displaying little PAP enveloping (Fig. 7).

We next performed a quantitative analysis of glial ensheathment. In WT neurons, ~90% of synapses had PAP ensheathment, both at 3–4 and 8–9 weeks (Fig. 8*a*). About 79–87% of these displayed ensheathment in both the spine and the presynaptic bouton, with the remaining 13–21% of synapses being ensheathed only in the spine or in the bouton (Fig. 8*a*). The overall percentage of synapses engulfed by PAPs was not substantially altered in Reelin-OE and Dab1-cKO mice (Fig. 8*c*). The percentage of ensheathed postsynaptic spines was also similar among the different groups and in different spine types (Fig. 8*d* and Supplementary Fig. 2). We found that 58–62% of spines in WT neurons were ensheathed in both the head and neck, with the remaining 28–32% of spines being ensheathed exclusively in the head or in the neck (Supplementary Fig. 2). Whereas the overexpression of Reelin resulted in a moderate decrease in the global ensheathment, Dab1-deficient neurons showed a marked increase in enwrapping and a greater percentage (67–89%) of spines engulfed in both the neck and spine (Supplementary Fig. 2). Regarding presynaptic partners, both overexpression and downregulation of Reelin led to a transient increase (35% and 31%, respectively) in the percentage of boutons ensheathed by PAPs at 3–4 weeks; at 8–9 weeks boutons in Dab1-KO neurons tended to have higher percentages (~95%), and, conversely, Reelin-OE neurons displayed lower percentages (70%) when compared with WT neurons (~89%) (Fig. 8*d*). These features were observed in both SSBs and MSBs.

The above findings suggested that Dab1-inactivation results in increased percentages of ensheathed synapses and that Reelin-OE leads to decreased astroglial ensheathment. We next measured the synaptic perimeter juxtaposed with astroglial processes at evenly distributed slices for completely imaged

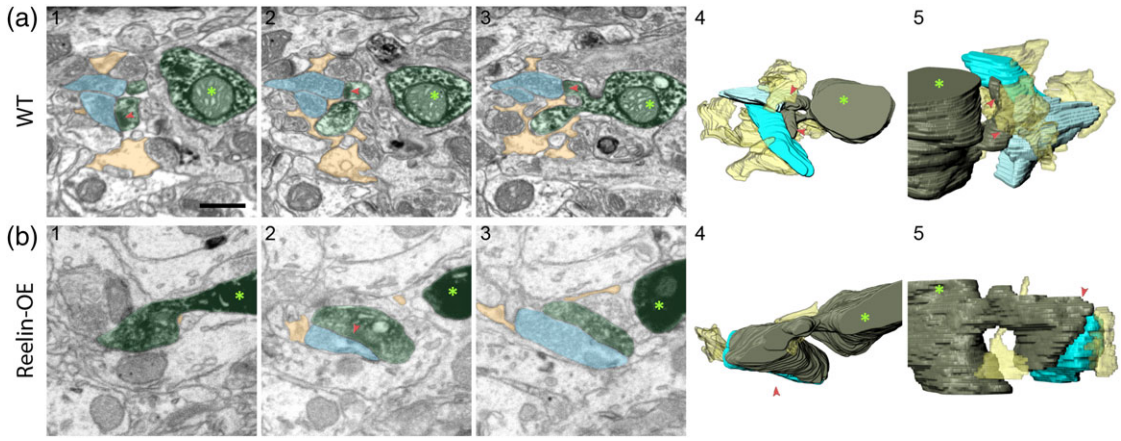

Figure 7. Astrocytic ensheathment of GC synapses in WT and Reelin-OE genotypes. Examples of synaptic couples enwrapped by PAPs in WT (*a*) and Reelin-OE (*b*) mice. The left images (1–3) show selected serial planes of PAPs (colored in yellow) surrounding the spines from 8- to 9-week GCs (colored in green, asterisk indicates the dendritic shaft) that establish synaptic contacts (red arrowheads) with presynaptic boutons (colored in blue). The right 3D reconstructions (4–5) show the astrocytic ensheathment in different orientations (yellow). Scale bar in *a*1 is 0.5 μm and applies for all panels.

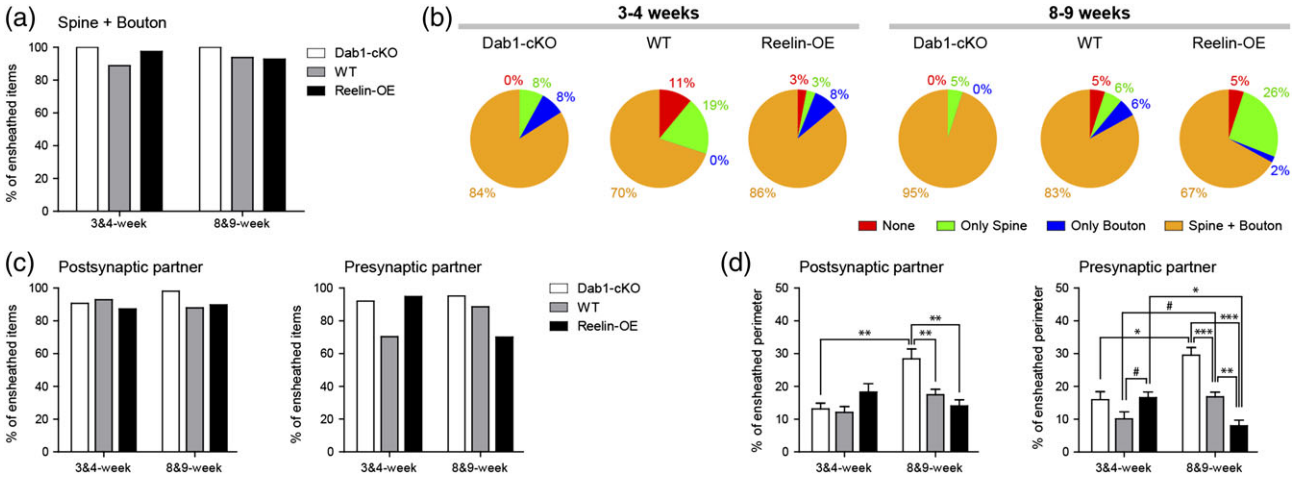

Figure 8. The Reelin/Dab1 pathway regulates the astroglial ensheathment of newborn GC synapses. (*a*) Proportion of synapses (spines+boutons) ensheathed by PAPs in 3–4 and 8- to 9-week-old WT, Reelin-OE, and Dab1-KO genotypes. (*b*) Round graphs showing the frequency of the different types of astrocytic ensheathment on synapses (only on the postsynaptic spine, only on the presynaptic bouton, or on both) of newborn WT, Reelin-OE, and Dab1-KO GCs at 3–4 and 8–9 weeks. (*c*) Proportion of postsynaptic spines and presynaptic boutons ensheathed by PAPs at 3–4 and 8–9-week-old WT, Reelin-OE, and Dab1-KO genotypes. (*d*) Percentage of the perimeter covered by astrocytic processes on spines and boutons at 3–4 and 8- to 9-week-old WT, Reelin-OE, and Dab1-KO genotypes. Data represent mean ± SEM. $^{*}P < 0.05$, $^{**}P < 0.01$, $^{***}P < 0.001$; Kruskal–Wallis test and post hoc Dunn's. $^{\#}P < 0.05$; Mann–Whitney test.

spines in 3D. About 12–17% of the spine perimeter in WT neurons was apposed to PAPs at 3–4 and 8–9 weeks, respectively (Fig. 8*d*). Dab1-inactivation led to a marked 63% increase in the ensheathment of GC spines, which accounted for all types of spines, and Reelin-OE neurons tended to show decreased, though non-significantly, glial ensheathment at 8 weeks (Fig. 8*d* and Supplementary Fig. 2). In contrast, at 3–4 weeks mushroom spines in Reelin-OE neurons displayed a sharp 96% increase in the ensheathed perimeter (Supplementary Fig. 2), suggesting that astrocytes contribute to the formation or stabilization of these spines. Analyses of ensheathment in presynaptic boutons at 8–9 weeks revealed that whereas Dab1-inactivation results in a clear ensheathment increase (76%), Reelin-OE leads to a significant decrease (–52%) (Fig. 8*d*). These differences held true for both SSBs and MSBs presynaptic to labeled GCs. Finally, at 3–4 weeks we found a higher presynaptic ensheathment in the SSBs of both Dab1-cKO and Reelin-OE mice with respect to WT (344% and 374%, respectively; Supplementary Fig. 2). Taken together, our results reveal that the Reelin/Dab1 pathway contributes to the fine tuning of the density of perisynaptic astroglial ensheathment of synapses established on newborn GCs, with overactivation of the pathway resulting in reduced ensheathment and Reelin-downregulation leading to increased ensheathment.

Discussion

Whereas the role of Reelin in spine and synaptic development has been well established by both in vivo studies in "reeler" and in neuronal cultures (Borrell et al. 1999; Liu et al. 2001; Qiu and Weeber 2007; Niu et al. 2008; Ventruti et al. 2011; Rogers et al. 2013), the role of Reelin in adult spine stability and remodeling is less well established. Whereas the overexpression of Reelin leads to spine hypertrophy, but not to spine density changes (Pujadas et al. 2010; Bosch et al. 2016), Reelin overexpression is sufficient to recover spine deficits in an

Alzheimer's disease mouse model (Pujadas et al. 2014), and Reelin infusions increase spine densities in CA1 WT neurons (Rogers et al. 2011) but not so in heterozygous reeler mice (Rogers et al. 2013). By using high resolution imaging techniques, we show in the present study that the Reelin/Dab1 pathway contributes to the regulation of the shapes and types of spines, to the complexity of their synapses and to the astrocytic perisynaptic ensheathment, indicating that the Reelin pathway is involved in the integration of newborn GCs in the preexisting circuit.

Taking advantage of retroviral markers, gain- and loss-of-function models, and 3D-microscopy techniques, we addressed how Reelin influences spine formation and connectivity in young-adult-generated GCs. Two-month aged mice were selected for retroviral injections by several reasons: First, 2-month-old young-adult mice correspond to 16–20-year-old humans (Finlay and Darlington 1995; Workman et al. 2013; Brust et al. 2015; Shoji et al. 2016) with the age of analysis (3- to 4-month-old mice) corresponding to adult humans. And second, injections in 2-month aged mice allow sufficient amount of retrovirally-labeled newborn GCs (Garthe et al. 2009; Krzisch et al. 2015; Mu et al. 2015; Restivo et al. 2015). Our results show that the overexpression of Reelin does not alter the pattern of spine formation and their densities in newborn GCs. In contrast, Dab1 downregulation leads to a transient increase in spine numbers at 4 weeks, which returns to numbers identical to those in WT neurons at 8 weeks. Thus, whereas over-activation of the Reelin pathway is not sufficient to alter the number of synaptic inputs to GCs, the downregulation of this signaling pathway increases the density of spines and presumed PSD95 contacts at early stages of GC maturation. To our knowledge this is the first study reporting that downregulation of the Reelin/Dab1 pathway increases spine numbers. It has been described that newborn GC display an increase of spines during their immature stages in some pathological conditions, such as stroke (Niv et al. 2012), epilepsy (Murphy et al. 2011), or inflammation (Chugh et al. 2013). Since these immature neurons are believed to have an important role in hippocampal function, it is possible that such spine increase in the absence of Reelin/Dab1 signaling might favor seizure-like episodes. Moreover, a study focused on layer 2/3 pyramidal neurons reported reduced spine density and enhanced adult Reelin expression linked to increased maternal care during their offspring (Smit-Rigter et al. 2009) and it has been reported that Autism Spectrum Disorder patients exhibit larger spine densities (Tang et al. 2014), with Reelin being a risk factor for this disease (Wang et al. 2014). Considering the positive role of Reelin in spine development (Qiu and Weeber 2007; Niu et al. 2008) and the different effects found in the adult (see above references), our findings suggest that the regulation of spinogenesis by Reelin may depend on the neuronal type analyzed and on developmental/adult stages, suggesting differential activation of signaling pathways downstream of Dab1.

A major effect of Reelin in the DG relies on spine morphology, type, and size. GCs in Reelin-OE mice exhibited a greater number of mushroom spines at both ages and a transient decrease in filopodial spines, and Reelin-OE mice exhibited both larger spines and synaptic contacts. Given current views on the shape of spines for their physiological and integrative properties, the relationship between mushroom spines with increased postsynaptic response and Long Term Potentiation (LTP) (Rusakov et al. 1996; Yuste and Majewska 2001; Matsuzaki et al. 2004; Harris and Weinberg 2012; Rochefort and Konnerth 2012), and findings highlighting a role for the "stronger" synapses in functional connectivity (Lefort et al. 2009; Cossell et al. 2015), our findings suggest greater excitability in Reelin-OE GCs. The increase in synaptic size in Reelin-OE mice would further enhance excitability since larger synapses contain higher numbers of AMPA receptors (Nusser et al. 1998; Takumi et al. 1999; Tarusawa et al. 2009), thus having a direct influence in postsynaptic strength (Montes et al. 2015). This agrees with studies reporting that Reelin potentiates glutamatergic neurotransmission and LTP (Weeber et al. 2002; Beffert et al. 2005; Qiu et al. 2006; Qiu and Weeber 2007; Pujadas et al. 2010; Rogers et al. 2011, 2013).

The main target of Dab1 downregulation in newborn GCs is once again mushroom spines; whereas at 8 weeks these spines were clearly decreased, there was a transient increase at 4 weeks, an age at which a reduction in thin spines occurred concomitant with a premature increase in branched spines. Synaptic contacts in Dab1-inactivated GCs were also smaller than in WT neurons. Together with the above findings in Reelin-OE mice, it is likely that mushroom spine emergence and stability is a primary target of the Reelin pathway. In addition, the strong multifaceted alterations found at 4 weeks in Dab1-deficient neurons, together with the increase in spine densities, suggest that Dab1 downregulation targets immature GC function and physiology by incrementing the hyperexcitability described for immature GCs (Ge et al. 2007). This could entail pathological consequences since hyperexcitability of the DG is one of the main characteristics of epilepsy (Murphy et al. 2011; Pun et al. 2012; Althaus et al. 2015), a pathology linked to low Reelin levels and to GC basal dendrites as in the Dab1-cKO model (Teixeira et al. 2012). Moreover, an immature hyperexcitable DG could be an endophenotype of psychiatric diseases (Yamasaki et al. 2008; Gu et al. 2012; Marin-Burgin et al. 2012; Shin et al. 2013; Zhou et al. 2013), pathologies that display low Reelin levels (Knable et al. 2004; Veldic et al. 2004).

A major target of Reelin in GC synaptogenesis was on the presynaptic terminals contacting with these neurons. In both Reelin-OE and Dab1-inactivated mice, axons innervating spines from newborn GCs established simultaneous synaptic contacts with fewer additional spines, indicating that Reelin deregulation in either direction alters such synaptic architecture. MSBs in the DG have been associated with plasticity and LTP and with mechanisms that may drive coactive synaptic activity, synchronous networks and rhythms (Harris 1995; Toni et al. 1999; Geinisman et al. 2001; Knott et al. 2006; Medvedev et al. 2014; Bosch et al. 2015). It is thus likely that both the overexpression and the downregulation of the Reelin pathway may lead to altered synchronicity and rhythms, which are important for cognitive processes, including learning and memory (Deng et al. 2010; Aimone et al. 2011; Buzsaki and Moser 2013). We report here that the Reelin/Dab1 pathway influences presynaptic synaptogenesis and presynaptic architecture, which raises several interesting mechanistic issues. In Reelin-OE mice, the simplest explanation is that extracellular Reelin may act directly on boutons, which express Reelin receptors (Bal et al. 2013) and Dab1 (Trotter et al. 2013); in fact, presynaptic boutons in reeler mice have been found to exhibit deficits in VAMP2/SNAP25 expression (Hellwig et al. 2011; Bal et al. 2013). However, the mechanism implicated in Dab1-inactivated GCs is likely to act indirectly, as the Reelin/Dab1 pathway was exclusively downregulated in the RV-infected GCs. This suggests the existence of Reelin-mediated indirect communicating mechanisms that may be disrupted in Dab1-deficient neurons. Such a mechanism would imply that either the postsynaptic neuron directly influences the multi-innervation complexity of the presynaptic axon, or else does so indirectly through adjacent cells

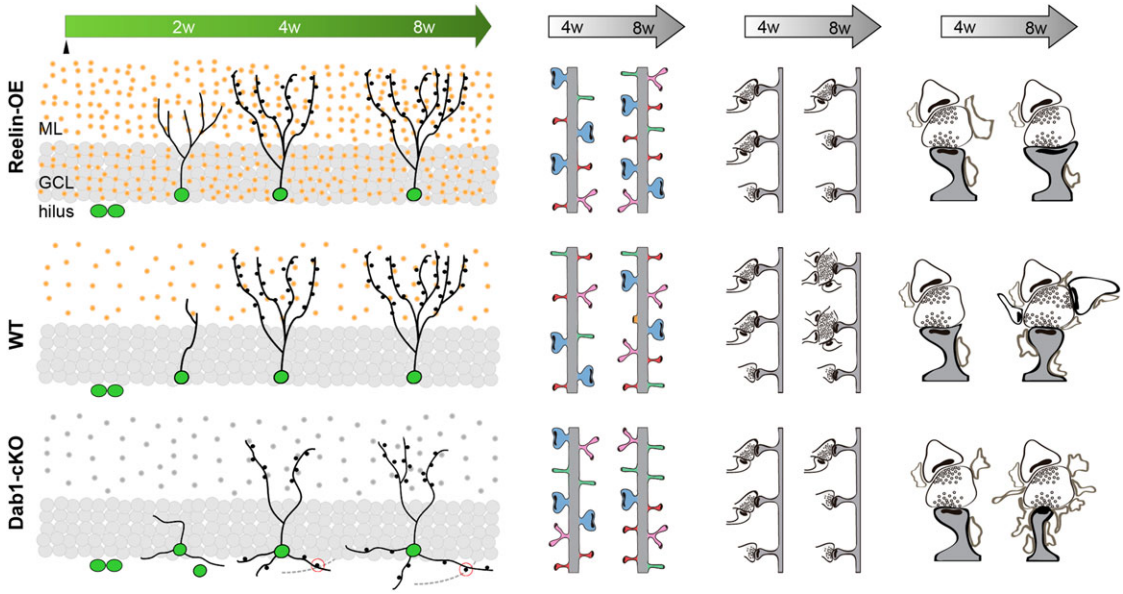

Figure 9. The Reelin/Dab1 pathway regulates dendritic, spine, and presynaptic development in young-adult-generated GCs. Representative diagram of adult neurogenesis in WT DG (center, left) shows Reelin presence in the ML of the DG (orange dots) and how new neurons increase their dendritic complexity and spine density over time. Gain of function of Reelin (top left) accelerates the growth of the dendritic tree of new GCs (green) without affecting their final morphology. Loss of Reelin signaling (gray dots) leads to the formation of aberrant granular cells, which possess a less complex dendritic tree in the ML and project several basal dendrites into the hilus, where they receive excitatory inputs (bottom left). Spines in WT experience changes in density and morphology from 4 to 8 w, and maturation occurs along with an increase in the presence of branched spines (central panels). Overexpression of Reelin does not change their density but it triggers a larger presence of mushroom spines at both 4 and 8 w (top). Dab1-cKO neurons exhibit a transient increase in dendritic spines at 4 w, but at 8 w no differences are present compared with WT. Loss of Dab1 leads to major changes in spine morphology, including a transient increase in mushroom and branched spines at 4 w, followed by a marked decrease in mushroom spines at 8 weeks and an increase in the filopodial type (bottom). Regarding the presynaptic bouton, the increase in synaptic multinnervation seen in WT from 4 to 8 weeks is severely disrupted upon both Reelin overexpression and Dab1 loss of function. Finally, downregulation or overactivation of the Reelin/Dab1 pathway leads to severe alterations in the perisynaptic astroglial ensheathment (right). Abbreviations: *GCL*, Granule Cell Layer.

such as astrocytes, whose activity plays a major role in spine development in GCs (Krzisch et al. 2015).

We show for the first time that Reelin regulates the extension of perisynaptic astroglial ensheathment. We found similar ensheathment in the control group as described previously for newborn GCs in the DG (Krzisch et al. 2015). However, whereas Reelin downregulation results in increased ensheathment of GC synapses, Reelin overexpression has the opposite effect. Recent evidence indicates that synaptic glial ensheathment is important in the control of synaptic homeostasis and excitability: not only do astrocyte synaptic processes contribute to neurotransmitter removal, thus preventing hyperexcitatability, but there is also increasing evidence of their role in synaptic plasticity, spine and synaptic development, and neuron/glial neurotransmission (Pfrieger and Barres 1997; Eroglu and Barres 2010; Bernardinelli et al. 2014b; Rothstein et al. 1996; Araque et al. 2014; Perez-Alvarez et al. 2014; Haydon and Nedergaard 2015; Sultan et al. 2015). It is thus tempting to speculate that, by modulating the degree of astrogial ensheathment, the Reelin pathway may contribute to at least some of these important processes. This also raises the possibility that the Reelin cascade may interact functionally with astrocyte-secreted signaling proteins such as Hevin and SPARC, that have been found to regulate synaptogenesis (Kucukdereli et al. 2011). However, further experiments would be required to establish a functional link between the structural changes here described and their physiological synaptic implications.

Together with our previous studies (Teixeira et al. 2012), our findings show that Reelin markedly regulates dendritic and synaptic maturation of newborn GCs. Whereas the overexpression of Reelin leads to accelerated dendritic maturation and to larger spines and synapses, and increased numbers of mushroom spines, the downregulation of the Reelin/Dab1 pathway leads to dendritic architecture alterations, synaptic circuit reorganization, increased spine density at 4 weeks, major changes in spine types at both 4 and 8 weeks, and smaller synapses at 8 weeks. In addition, both the downregulation and the overexpression of the Reelin cascade result in a decrease in MSB synaptic innervation (Fig. 9). Lastly, the Reelin/Dab1 pathway controls the extension of astroglial ensheathment in newborn GC synapses. Thus, Reelin regulates distinct steps of GC maturation, including dendritogenesis and dendritic orientation, dendritic spinogenesis and synaptogenesis, and astroglial ensheathment, which is likely to be transduced in profound changes in the electrical properties of GCs and in the network activity in which they are recruited. Interestingly, both overexpression and downregulation of the Reelin/Dab1 pathway led to dramatic connectivity and glial ensheathment alterations, indicating that fine, precise control of Reelin expression is needed for the correct maturation and functional integration of young-adult-born GCs. Given the influence of Reelin in neurodegenerative and psychiatric diseases and in epilepsy (Guidotti et al. 2000; Dutta et al. 2011; Folsom and Fatemi 2013; Notter and Knuesel 2013), we propose that the alterations here described may contribute to the pathogenic traits associated with these diseases.

Supplementary Material

Supplementary material can be found at: http://www.cercor.oxfordjournals.org/.

Funding

Spanish MINECO (BFU 2008-03980 and SAF 2013-42445R to ES, SAF 2013-2010-19930 and PIE 13-00027 to JXC, and SAF 2015-66603-P to JdF); CIBERNED (to ES, JC, and JdF), the Cajal Blue Brain Project; Spanish partner of the Blue Brain Project initiative from EPFL (to JdF); the European Union Seventh Framework Programme (FP7/2007-2013) (grant agreement no. 604102) (Human Brain Project) (to JdF); Generalitat de Catalunya (SGR and ICREA Academia).

Notes

We thank Tanya Yates and Tom Yohannan for editorial assistance, Jorge G Peña for the EspINA software development and Alfonso Pérez-Escudero for critical discussion. *Conflict of Interest*: None declared.

References

Abdolmaleky HM, Cheng KH, Russo A, Smith CL, Faraone SV, Wilcox M, Shafa R, Glatt SJ, Nguyen G, Ponte JF, et al. 2005. Hypermethylation of the reelin (RELN) promoter in the brain of schizophrenic patients: a preliminary report. Am J Med Genet B Neuropsychiatr Genet. 134B:60–66.

Aimone JB, Deng W, Gage FH. 2011. Resolving new memories: a critical look at the dentate gyrus, adult neurogenesis, and pattern separation. Neuron. 70:589–596.

Akers KG, Martinez-Canabal A, Restivo L, Yiu AP, De Cristofaro A, Hsiang HL, Wheeler AL, Guskjolen A, Niibori Y, Shoji H, et al. 2014. Hippocampal neurogenesis regulates forgetting during adulthood and infancy. Science. 344:598–602.

Alcantara S, Ruiz M, D'Arcangelo G, Ezan F, de Lecea L, Curran T, Sotelo C, Soriano E. 1998. Regional and cellular patterns of reelin mRNA expression in the forebrain of the developing and adult mouse. J Neurosci. 18:7779–7799.

Althaus AL, Sagher O, Parent JM, Murphy GG. 2015. Intrinsic neurophysiological properties of hilar ectopic and normotopic dentate granule cells in human temporal lobe epilepsy and a rat model. J Neurophysiol. 113:1184–1194.

Andersen P, Morris R, Amaral D, Bliss T, O'Keefe J. 2007. The Hippocampus Book. New York: Oxford University Press.

Araque A, Carmignoto G, Haydon PG, Oliet SH, Robitaille R, Volterra A. 2014. Gliotransmitters travel in time and space. Neuron. 81:728–739.

Arellano JI, Benavides-Piccione R, Defelipe J, Yuste R. 2007. Ultrastructure of dendritic spines: correlation between synaptic and spine morphologies. Front Neurosci. 1:131–143.

Arnaud L, Ballif BA, Forster E, Cooper JA. 2003. Fyn tyrosine kinase is a critical regulator of disabled-1 during brain development. Curr Biol. 13:9–17.

Bal M, Leitz J, Reese AL, Ramirez DM, Durakoglugil M, Herz J, Monteggia LM, Kavalali ET. 2013. Reelin mobilizes a VAMP7-dependent synaptic vesicle pool and selectively augments spontaneous neurotransmission. Neuron. 80:934–946.

Ballif BA, Arnaud L, Arthur WT, Guris D, Imamoto A, Cooper JA. 2004. Activation of a Dab1/CrkL/C3G/Rap1 pathway in Reelin-stimulated neurons. Curr Biol. 14:606–610.

Beffert U, Morfini G, Bock HH, Reyna H, Brady ST, Herz J. 2002. Reelin-mediated signaling locally regulates protein kinase B/Akt and glycogen synthase kinase 3beta. J Biol Chem. 277:49958–49964.

Beffert U, Weeber EJ, Durudas A, Qiu S, Masiulis I, Sweatt JD, Li WP, Adelmann G, Frotscher M, Hammer RE, et al. 2005. Modulation of synaptic plasticity and memory by Reelin involves differential splicing of the lipoprotein receptor Apoer2. Neuron. 47:567–579.

Benavides-Piccione R, Fernaud-Espinosa I, Robles V, Yuste R, DeFelipe J. 2013. Age-based comparison of human dendritic spine structure using complete three-dimensional reconstructions. Cereb Cortex. 23:1798–1810.

Bernardinelli Y, Muller D, Nikonenko I. 2014a. Astrocyte-synapse structural plasticity. Neural Plast. 2014:232105.

Bernardinelli Y, Randall J, Janett E, Nikonenko I, Konig S, Jones EV, Flores CE, Murai KK, Bochet CG, Holtmaat A, et al. 2014b. Activity-dependent structural plasticity of perisynaptic astrocytic domains promotes excitatory synapse stability. Curr Biol. 24:1679–1688.

Borrell V, Ruiz M, Del Rio JA, Soriano E. 1999. Development of commissural connections in the hippocampus of reeler mice: evidence of an inhibitory influence of Cajal-Retzius cells. Exp Neurol. 156:268–282.

Bosch C, Martinez A, Masachs N, Teixeira CM, Fernaud I, Ulloa F, Perez-Martinez E, Lois C, Comella JX, DeFelipe J, et al. 2015. FIB/SEM technology and high-throughput 3D reconstruction of dendritic spines and synapses in GFP-labeled adult-generated neurons. Front Neuroanat. 9:60.

Bosch C, Muhaisen A, Pujadas L, Soriano E, Martinez A. 2016. Reelin exerts structural, biochemical and transcriptional regulation over presynaptic and postsynaptic elements in the adult hippocampus. Front Cell Neurosci. 10:138.

Brust V, Schindler PM, Lewejohann L. 2015. Lifetime development of behavioural phenotype in the house mouse (Mus musculus). Front Zool. 12 (Suppl 1):S17.

Buzsaki G, Moser EI. 2013. Memory, navigation and theta rhythm in the hippocampal-entorhinal system. Nat Neurosci. 16:130–138.

Chen Y, Beffert U, Ertunc M, Tang TS, Kavalali ET, Bezprozvanny I, Herz J. 2005. Reelin modulates NMDA receptor activity in cortical neurons. J Neurosci. 25:8209–8216.

Cho KO, Lybrand ZR, Ito N, Brulet R, Tafacory F, Zhang L, Good L, Ure K, Kernie SG, Birnbaum SG, et al. 2015. Aberrant hippocampal neurogenesis contributes to epilepsy and associated cognitive decline. Nat Commun. 6:6606.

Chugh D, Nilsson P, Afjei SA, Bakochi A, Ekdahl CT. 2013. Brain inflammation induces post-synaptic changes during early synapse formation in adult-born hippocampal neurons. Exp Neurol. 250:176–188.

Clelland CD, Choi M, Romberg C, Clemenson GDJr, Fragniere A, Tyers P, Jessberger S, Saksida LM, Barker RA, Gage FH, et al. 2009. A functional role for adult hippocampal neurogenesis in spatial pattern separation. Science. 325:210–213.

Cooper JA. 2008. A mechanism for inside-out lamination in the neocortex. Trends Neurosci. 31:113–119.

Cossell L, Iacaruso MF, Muir DR, Houlton R, Sader EN, Ko H, Hofer SB, Mrsic-Flogel TD. 2015. Functional organization of excitatory synaptic strength in primary visual cortex. Nature. 518:399–403.

D'Arcangelo G, Miao GG, Chen SC, Soares HD, Morgan JI, Curran T. 1995. A protein related to extracellular matrix proteins deleted in the mouse mutant reeler. Nature. 374:719–723.

Dazzo E, Fanciulli M, Serioli E, Minervini G, Pulitano P, Binelli S, Di Bonaventura C, Luisi C, Pasini E, Striano S, et al. 2015. Heterozygous Reelin mutations cause autosomal-dominant lateral temporal epilepsy. Am J Hum Genet. 96:992–1000.

Deng W, Aimone JB, Gage FH. 2010. New neurons and new memories: how does adult hippocampal neurogenesis affect learning and memory?. Nat Rev Neurosci. 11:339–350.

Dutta S, Gangopadhyay PK, Sinha S, Chatterjee A, Ghosh S, Rajamma U. 2011. An association analysis of reelin gene (RELN) polymorphisms with childhood epilepsy in eastern Indian population from West Bengal. Cell Mol Neurobiol. 31:45–56.

Eroglu C, Barres BA. 2010. Regulation of synaptic connectivity by glia. Nature. 468:223–231.

Finlay BL, Darlington RB. 1995. Linked regularities in the development and evolution of mammalian brains. Science. 268:1578–1584.

Folsom TD, Fatemi SH. 2013. The involvement of Reelin in neurodevelopmental disorders. Neuropharmacology. 68:122–135.

Franco SJ, Martinez-Garay I, Gil-Sanz C, Harkins-Perry SR, Muller U. 2011. Reelin regulates cadherin function via Dab1/Rap1 to control neuronal migration and lamination in the neocortex. Neuron. 69:482–497.

Gao Z, Ure K, Ables JL, Lagace DC, Nave KA, Goebbels S, Eisch AJ, Hsieh J. 2009. Neurod1 is essential for the survival and maturation of adult-born neurons. Nat Neurosci. 12:1090–1092.

Garthe A, Behr J, Kempermann G. 2009. Adult-generated hippocampal neurons allow the flexible use of spatially precise learning strategies. PLoS One. 4:e5464.

Ge S, Yang CH, Hsu KS, Ming GL, Song H. 2007. A critical period for enhanced synaptic plasticity in newly generated neurons of the adult brain. Neuron. 54:559–566.

Geinisman Y, Berry RW, Disterhoft JF, Power JM, Van der Zee EA. 2001. Associative learning elicits the formation of multiple-synapse boutons. J Neurosci. 21:5568–5573.

Gonzalez-Billault C, Del Rio JA, Urena JM, Jimenez-Mateos EM, Barallobre MJ, Pascual M, Pujadas L, Simo S, Torre AL, Gavin R, et al. 2005. A role of MAP1B in Reelin-dependent neuronal migration. Cereb Cortex. 15:1134–1145.

Groc L, Choquet D, Stephenson FA, Verrier D, Manzoni OJ, Chavis P. 2007. NMDA receptor surface trafficking and synaptic subunit composition are developmentally regulated by the extracellular matrix protein Reelin. J Neurosci. 27:10165–10175.

Gu Y, Arruda-Carvalho M, Wang J, Janoschka SR, Josselyn SA, Frankland PW, Ge S. 2012. Optical controlling reveals time-dependent roles for adult-born dentate granule cells. Nat Neurosci. 15:1700–1706.

Guidotti A, Auta J, Davis JM, Di-Giorgi-Gerevini V, Dwivedi Y, Grayson DR, Impagnatiello F, Pandey G, Pesold C, Sharma R, et al. 2000. Decrease in reelin and glutamic acid decarboxylase67 (GAD67) expression in schizophrenia and bipolar disorder: a postmortem brain study. Arch Gen Psychiatry. 57:1061–1069.

Harris KM. 1995. How multiple-synapse boutons could preserve input specificity during an interneuronal spread of LTP. Trends Neurosci. 18:365–369.

Harris KM, Jensen FE, Tsao B. 1992. Three-dimensional structure of dendritic spines and synapses in rat hippocampus (CA1) at postnatal day 15 and adult ages: implications for the maturation of synaptic physiology and long-term potentiation. J Neurosci. 12:2685–2705.

Harris KM, Weinberg RJ. 2012. Ultrastructure of synapses in the mammalian brain. Cold Spring Harb Perspect Biol. 4:1–15.

Haydon PG, Nedergaard M. 2015. How do astrocytes participate in neural plasticity?. Cold Spring Harb Perspect Biol. 7: a020438.

Hellwig S, Hack I, Kowalski J, Brunne B, Jarowyj J, Unger A, Bock HH, Junghans D, Frotscher M. 2011. Role for Reelin in neurotransmitter release. J Neurosci. 31:2352–2360.

Herz J, Chen Y. 2006. Reelin, lipoprotein receptors and synaptic plasticity. Nat Rev Neurosci. 7:850–859.

Hiesberger T, Trommsdorff M, Howell BW, Goffinet A, Mumby MC, Cooper JA, Herz J. 1999. Direct binding of Reelin to VLDL receptor and ApoE receptor 2 induces tyrosine phosphorylation of disabled-1 and modulates tau phosphorylation. Neuron. 24:481–489.

Howell BW, Hawkes R, Soriano P, Cooper JA. 1997. Neuronal position in the developing brain is regulated by mouse disabled-1. Nature. 389:733–737.

Howell BW, Herrick TM, Cooper JA. 1999. Reelin-induced tyrosine [corrected] phosphorylation of disabled 1 during neuronal positioning. Genes Dev. 13:643–648.

Jessberger S, Toni N, Clemenson GDJr, Ray J, Gage FH. 2008. Directed differentiation of hippocampal stem/progenitor cells in the adult brain. Nat Neurosci. 11:888–893.

Karalay O, Doberauer K, Vadodaria KC, Knobloch M, Berti L, Miquelajauregui A, Schwark M, Jagasia R, Taketo MM, Tarabykin V, et al. 2011. Prospero-related homeobox 1 gene (Prox1) is regulated by canonical Wnt signaling and has a stage-specific role in adult hippocampal neurogenesis. Proc Natl Acad Sci USA. 108:5807–5812.

Kelsch W, Lin CW, Lois C. 2008. Sequential development of synapses in dendritic domains during adult neurogenesis. Proc Natl Acad Sci USA. 105:16803–16808.

Kheirbek MA, Klemenhagen KC, Sahay A, Hen R. 2012. Neurogenesis and generalization: a new approach to stratify and treat anxiety disorders. Nat Neurosci. 15:1613–1620.

Knable MB, Barci BM, Webster MJ, Meador-Woodruff J, Torrey EF, Stanley Neuropathology C. 2004. Molecular abnormalities of the hippocampus in severe psychiatric illness: postmortem findings from the Stanley Neuropathology Consortium. Mol Psychiatry. 9:609–620, 544.

Knott GW, Holtmaat A, Wilbrecht L, Welker E, Svoboda K. 2006. Spine growth precedes synapse formation in the adult neocortex in vivo. Nat Neurosci. 9:1117–1124.

Knuesel I. 2010. Reelin-mediated signaling in neuropsychiatric and neurodegenerative diseases. Prog Neurobiol. 91:257–274.

Krstic D, Knuesel I. 2013. Deciphering the mechanism underlying late-onset Alzheimer disease. Nat Rev Neurol. 9:25–34.

Krzisch M, Temprana SG, Mongiat LA, Armida J, Schmutz V, Virtanen MA, Kocher-Braissant J, Kraftsik R, Vutskits L, Conzelmann KK, et al. 2015. Pre-existing astrocytes form functional perisynaptic processes on neurons generated in the adult hippocampus. Brain Struct Funct. 220:2027–2042.

Kucukdereli H, Allen NJ, Lee AT, Feng A, Ozlu MI, Conatser LM, Chakraborty C, Workman G, Weaver M, Sage EH, et al. 2011. Control of excitatory CNS synaptogenesis by astrocyte-secreted proteins Hevin and SPARC. Proc Natl Acad Sci USA. 108:E440–E449.

Lagace DC, Benavides DR, Kansy JW, Mapelli M, Greengard P, Bibb JA, Eisch AJ. 2008. Cdk5 is essential for adult hippocampal neurogenesis. Proc Natl Acad Sci USA. 105:18567–18571.

Lefort S, Tomm C, Floyd Sarria JC, Petersen CC. 2009. The excitatory neuronal network of the C2 barrel column in mouse primary somatosensory cortex. Neuron. 61:301–316.

Lemaire V, Tronel S, Montaron MF, Fabre A, Dugast E, Abrous DN. 2012. Long-lasting plasticity of hippocampal adult-born neurons. J Neurosci. 32:3101–3108.

Lie DC, Colamarino SA, Song HJ, Desire L, Mira H, Consiglio A, Lein ES, Jessberger S, Lansford H, Dearie AR, et al. 2005. Wnt

signalling regulates adult hippocampal neurogenesis. Nature. 437:1370–1375.

Liu WS, Pesold C, Rodriguez MA, Carboni G, Auta J, Lacor P, Larson J, Condie BG, Guidotti A, Costa E. 2001. Down-regulation of dendritic spine and glutamic acid decarboxylase 67 expressions in the reelin haploinsufficient heterozygous reeler mouse. Proc Natl Acad Sci USA. 98:3477–3482.

Llorens-Martin M, Fuster-Matanzo A, Teixeira CM, Jurado-Arjona J, Ulloa F, Defelipe J, Rabano A, Hernandez F, Soriano E, Avila J. 2013. GSK-3beta overexpression causes reversible alterations on postsynaptic densities and dendritic morphology of hippocampal granule neurons in vivo. Mol Psychiatry. 18:451–460.

Marin-Burgin A, Mongiat LA, Pardi MB, Schinder AF. 2012. Unique processing during a period of high excitation/inhibition balance in adult-born neurons. Science. 335:1238–1242.

Martin R, Bajo-Graneras R, Moratalla R, Perea G, Araque A. 2015. GLIAL CELL SIGNALING. Circuit-specific signaling in astrocyte-neuron networks in basal ganglia pathways. Science. 349:730–734.

Matsuzaki M, Honkura N, Ellis-Davies GC, Kasai H. 2004. Structural basis of long-term potentiation in single dendritic spines. Nature. 429:761–766.

Medvedev NI, Dallerac G, Popov VI, Rodriguez Arellano JJ, Davies HA, Kraev IV, Doyere V, Stewart MG. 2014. Multiple spine boutons are formed after long-lasting LTP in the awake rat. Brain Struct Funct. 219:407–414.

Merchan-Perez A, Rodriguez JR, Alonso-Nanclares L, Schertel A, Defelipe J. 2009. Counting synapses using FIB/SEM microscopy: a true revolution for ultrastructural volume reconstruction. Front Neuroanat. 3:18.

Montes J, Pena JM, DeFelipe J, Herreras O, Merchan-Perez A. 2015. The influence of synaptic size on AMPA receptor activation: a Monte Carlo model. PLoS One. 10:e0130924.

Moon UY, Park JY, Park R, Cho JY, Hughes LJ, McKenna JIII, Goetzl L, Cho SH, Crino PB, Gambello MJ, et al. 2015. Impaired Reelin-Dab1 signaling contributes to neuronal migration deficits of tuberous sclerosis complex. Cell Rep. 12:965–978.

Morales J, Alonso-Nanclares L, Rodriguez JR, Defelipe J, Rodriguez A, Merchan-Perez A. 2011. Espina: a tool for the automated segmentation and counting of synapses in large stacks of electron microscopy images. Front Neuroanat. 5:18.

Mu Y, Zhao C, Toni N, Yao J, Gage FH. 2015. Distinct roles of NMDA receptors at different stages of granule cell development in the adult brain. Elife. 4:e07871.

Murphy BL, Pun RY, Yin H, Faulkner CR, Loepke AW, Danzer SC. 2011. Heterogeneous integration of adult-generated granule cells into the epileptic brain. J Neurosci. 31:105–117.

Niu S, Yabut O, D'Arcangelo G. 2008. The Reelin signaling pathway promotes dendritic spine development in hippocampal neurons. J Neurosci. 28:10339–10348.

Niv F, Keiner S, Krishna, Witte OW, Lie DC, Redecker C. 2012. Aberrant neurogenesis after stroke: a retroviral cell labeling study. Stroke. 43:2468–2475.

Notter T, Knuesel I. 2013. Reelin immunoreactivity in neuritic varicosities in the human hippocampal formation of non-demented subjects and Alzheimer's disease patients. Acta Neuropathol Commun. 1:27.

Nusser Z, Lujan R, Laube G, Roberts JD, Molnar E, Somogyi P. 1998. Cell type and pathway dependence of synaptic AMPA receptor number and variability in the hippocampus. Neuron. 21:545–559.

Perez-Alvarez A, Navarrete M, Covelo A, Martin ED, Araque A. 2014. Structural and functional plasticity of astrocyte processes and dendritic spine interactions. J Neurosci. 34:12738–12744.

Peters A, Palay S. 1991. The Fine Structure of the Nervous System: neurons and Their Supporting Cells. New York: Oxford University Press.

Pfrieger FW, Barres BA. 1997. Synaptic efficacy enhanced by glial cells in vitro. Science. 277:1684–1687.

Pramatarova A, Chen K, Howell BW. 2008. A genetic interaction between the APP and Dab1 genes influences brain development. Mol Cell Neurosci. 37:178–186.

Pujadas L, Gruart A, Bosch C, Delgado L, Teixeira CM, Rossi D, de Lecea L, Martinez A, Delgado-Garcia JM, Soriano E. 2010. Reelin regulates postnatal neurogenesis and enhances spine hypertrophy and long-term potentiation. J Neurosci. 30:4636–4649.

Pujadas L, Rossi D, Andres R, Teixeira CM, Serra-Vidal B, Parcerisas A, Maldonado R, Giralt E, Carulla N, Soriano E. 2014. Reelin delays amyloid-beta fibril formation and rescues cognitive deficits in a model of Alzheimer's disease. Nat Commun. 5:3443.

Pun RY, Rolle IJ, Lasarge CL, Hosford BE, Rosen JM, Uhl JD, Schmeltzer SN, Faulkner C, Bronson SL, Murphy BL, et al. 2012. Excessive activation of mTOR in postnatally generated granule cells is sufficient to cause epilepsy. Neuron. 75:1022–1034.

Qiu S, Weeber EJ. 2007. Reelin signaling facilitates maturation of CA1 glutamatergic synapses. J Neurophysiol. 97:2312–2321.

Qiu S, Zhao LF, Korwek KM, Weeber EJ. 2006. Differential reelin-induced enhancement of NMDA and AMPA receptor activity in the adult hippocampus. J Neurosci. 26:12943–12955.

Restivo L, Niibori Y, Mercaldo V, Josselyn SA, Frankland PW. 2015. Development of adult-generated cell connectivity with excitatory and inhibitory cell populations in the hippocampus. J Neurosci. 35:10600–10612.

Rice DS, Curran T. 2001. Role of the reelin signaling pathway in central nervous system development. Annu Rev Neurosci. 24:1005–1039.

Rochefort NL, Konnerth A. 2012. Dendritic spines: from structure to in vivo function. EMBO Rep. 13:699–708.

Rogers JT, Rusiana I, Trotter J, Zhao L, Donaldson E, Pak DT, Babus LW, Peters M, Banko JL, Chavis P, et al. 2011. Reelin supplementation enhances cognitive ability, synaptic plasticity, and dendritic spine density. Learn Mem. 18:558–564.

Rogers JT, Zhao L, Trotter JH, Rusiana I, Peters MM, Li Q, Donaldson E, Banko JL, Keenoy KE, Rebeck GW, et al. 2013. Reelin supplementation recovers sensorimotor gating, synaptic plasticity and associative learning deficits in the heterozygous reeler mouse. J Psychopharmacol. 27: 386–395.

Rothstein JD, Dykes-Hoberg M, Pardo CA, Bristol LA, Jin L, Kuncl RW, Kanai Y, Hediger MA, Wang Y, Schielke JP, et al. 1996. Knockout of glutamate transporters reveals a major role for astroglial transport in excitotoxicity and clearance of glutamate. Neuron. 16:675–686.

Rusakov DA, Stewart MG, Korogod SM. 1996. Branching of active dendritic spines as a mechanism for controlling synaptic efficacy. Neuroscience. 75:315–323.

Sahay A, Scobie KN, Hill AS, O'Carroll CM, Kheirbek MA, Burghardt NS, Fenton AA, Dranovsky A, Hen R. 2011. Increasing adult hippocampal neurogenesis is sufficient to improve pattern separation. Nature. 472:466–470.

Schindelin J, Arganda-Carreras I, Frise E, Kaynig V, Longair M, Pietzsch T, Preibisch S, Rueden C, Saalfeld S, Schmid B, et al.

2012. Fiji: an open-source platform for biological-image analysis. Nat Methods. 9:676–682.

Sheldon M, Rice DS, D'Arcangelo G, Yoneshima H, Nakajima K, Mikoshiba K, Howell BW, Cooper JA, Goldowitz D, Curran T. 1997. Scrambler and yotari disrupt the disabled gene and produce a reeler-like phenotype in mice. Nature. 389:730–733.

Shin R, Kobayashi K, Hagihara H, Kogan JH, Miyake S, Tajinda K, Walton NM, Gross AK, Heusner CL, Chen Q, et al. 2013. The immature dentate gyrus represents a shared phenotype of mouse models of epilepsy and psychiatric disease. Bipolar Disord. 15:405–421.

Shoji H, Takao K, Hattori S, Miyakawa T. 2016. Age-related changes in behavior in C57BL/6J mice from young adulthood to middle age. Mol Brain. 9:11.

Simo S, Pujadas L, Segura MF, La Torre A, Del Rio JA, Urena JM, Comella JX, Soriano E. 2007. Reelin induces the detachment of postnatal subventricular zone cells and the expression of the Egr-1 through Erk1/2 activation. Cereb Cortex. 17:294–303.

Smit-Rigter LA, Champagne DL, van Hooft JA. 2009. Lifelong impact of variations in maternal care on dendritic structure and function of cortical layer 2/3 pyramidal neurons in rat offspring. PLoS One. 4:e5167.

Song J, Sun J, Moss J, Wen Z, Sun GJ, Hsu D, Zhong C, Davoudi H, Christian KM, Toni N, et al. 2013. Parvalbumin interneurons mediate neuronal circuitry-neurogenesis coupling in the adult hippocampus. Nat Neurosci. 16:1728–1730.

Soriano E, Del Rio JA. 2005. The cells of cajal-retzius: still a mystery one century after. Neuron. 46:389–394.

Sultan S, Li L, Moss J, Petrelli F, Casse F, Gebara E, Lopatar J, Pfrieger FW, Bezzi P, Bischofberger J, et al. 2015. Synaptic integration of adult-born hippocampal neurons is locally controlled by astrocytes. Neuron. 88:957–972.

Sun B, Halabisky B, Zhou Y, Palop JJ, Yu G, Mucke L, Gan L. 2009. Imbalance between GABAergic and glutamatergic transmission impairs adult neurogenesis in an animal model of Alzheimer's disease. Cell Stem Cell. 5:624–633.

Takumi Y, Ramirez-Leon V, Laake P, Rinvik E, Ottersen OP. 1999. Different modes of expression of AMPA and NMDA receptors in hippocampal synapses. Nat Neurosci. 2:618–624.

Tang G, Gudsnuk K, Kuo SH, Cotrina ML, Rosoklija G, Sosunov A, Sonders MS, Kanter E, Castagna C, Yamamoto A, et al. 2014. Loss of mTOR-dependent macroautophagy causes autistic-like synaptic pruning deficits. Neuron. 83:1131–1143.

Tarusawa E, Matsui K, Budisantoso T, Molnar E, Watanabe M, Matsui M, Fukazawa Y, Shigemoto R. 2009. Input-specific intrasynaptic arrangements of ionotropic glutamate receptors and their impact on postsynaptic responses. J Neurosci. 29:12896–12908.

Teixeira CM, Kron MM, Masachs N, Zhang H, Lagace DC, Martinez A, Reillo I, Duan X, Bosch C, Pujadas L, et al. 2012. Cell-autonomous inactivation of the reelin pathway impairs adult neurogenesis in the hippocampus. J Neurosci. 32:12051–12065.

Teixeira CM, Masachs N, Muhaisen A, Bosch C, Perez-Martinez J, Howell B, Soriano E. 2014. Transient downregulation of Dab1 protein levels during development leads to behavioral and structural deficits: relevance for psychiatric disorders. Neuropsychopharmacology. 39:556–568.

Toni N, Buchs PA, Nikonenko I, Bron CR, Muller D. 1999. LTP promotes formation of multiple spine synapses between a single axon terminal and a dendrite. Nature. 402:421–425.

Toni N, Teng EM, Bushong EA, Aimone JB, Zhao C, Consiglio A, van Praag H, Martone ME, Ellisman MH, Gage FH. 2007. Synapse formation on neurons born in the adult hippocampus. Nat Neurosci. 10:727–734.

Trotter J, Lee GH, Kazdoba TM, Crowell B, Domogauer J, Mahoney HM, Franco SJ, Muller U, Weeber EJ, D'Arcangelo G. 2013. Dab1 is required for synaptic plasticity and associative learning. J Neurosci. 33:15652–15668.

Vadodaria KC, Gage FH. 2014. SnapShot: adult hippocampal neurogenesis. Cell. 156:1114.

Veldic M, Caruncho HJ, Liu WS, Davis J, Satta R, Grayson DR, Guidotti A, Costa E. 2004. DNA-methyltransferase 1 mRNA is selectively overexpressed in telencephalic GABAergic interneurons of schizophrenia brains. Proc Natl Acad Sci USA. 101:348–353.

Ventruti A, Kazdoba TM, Niu S, D'Arcangelo G. 2011. Reelin deficiency causes specific defects in the molecular composition of the synapses in the adult brain. Neuroscience. 189:32–42.

Wang Z, Hong Y, Zou L, Zhong R, Zhu B, Shen N, Chen W, Lou J, Ke J, Zhang T, et al. 2014. Reelin gene variants and risk of autism spectrum disorders: an integrated meta-analysis. Am J Med Genet B Neuropsychiatr Genet. 165B:192–200.

Weeber EJ, Beffert U, Jones C, Christian JM, Forster E, Sweatt JD, Herz J. 2002. Reelin and ApoE receptors cooperate to enhance hippocampal synaptic plasticity and learning. J Biol Chem. 277:39944–39952.

Workman AD, Charvet CJ, Clancy B, Darlington RB, Finlay BL. 2013. Modeling transformations of neurodevelopmental sequences across mammalian species. J Neurosci. 33: 7368–7383.

Yamasaki N, Maekawa M, Kobayashi K, Kajii Y, Maeda J, Soma M, Takao K, Tanda K, Ohira K, Toyama K, et al. 2008. Alpha-CaMKII deficiency causes immature dentate gyrus, a novel candidate endophenotype of psychiatric disorders. Mol Brain. 1:6.

Yu DX, Marchetto MC, Gage FH. 2014. How to make a hippocampal dentate gyrus granule neuron. Development. 141:2366–2375.

Yuste R, Majewska A. 2001. On the function of dendritic spines. Neuroscientist. 7:387–395.

Zhao C, Deng W, Gage FH. 2008. Mechanisms and functional implications of adult neurogenesis. Cell. 132:645–660.

Zhao C, Jou J, Wolff LJ, Sun H, Gage FH. 2014. Spine morphogenesis in newborn granule cells is differentially regulated in the outer and middle molecular layers. J Comp Neurol. 522:2756–2766.

Zhao C, Teng EM, Summers RGJr, Ming GL, Gage FH. 2006. Distinct morphological stages of dentate granule neuron maturation in the adult mouse hippocampus. J Neurosci. 26:3–11.

Zhou M, Li W, Huang S, Song J, Kim JY, Tian X, Kang E, Sano Y, Liu C, Balaji J, et al. 2013. mTOR Inhibition ameliorates cognitive and affective deficits caused by Disc1 knockdown in adult-born dentate granule neurons. Neuron. 77:647–654.